RSC Applied Polymers

ROYAL SOCIETY OF CHEMISTRY

REVIEW

View Article Online
View Journal | View Issue

Cite this: *RSC Appl. Polym.*, 2025, **3**, 1403

Nanocarrier strategies for deep tumour penetration

Jinbo Zhang, Guanjiang Wu and Valentin A. Bobrin *

Received 27th May 2025,
Accepted 8th August 2025

DOI: 10.1039/d5lp00154d

rsc.li/rscapplpolym

Deep penetration of nanocarriers into solid tumours remains a major obstacle in cancer nanomedicine due to the complex tumour microenvironment (TME) and associated physiological barriers. This review provides a comprehensive analysis to guide the design of stimuli-responsive nanocarriers capable of overcoming these transport limitations and enhancing therapeutic efficacy. It begins by examining key nanocarrier classes, including lipid-based, polymeric, inorganic, biomacromolecular, and hydrogel systems, highlighting their structural features, advantages, and limitations. Special focus is given to charge-reversal nanoparticles, which leverage TME-specific triggers such as acidic pH, redox gradients, and enzymatic activity to enhance tumour infiltration and cellular uptake. The review also evaluates complementary strategies including size and shape transformation, surface ligand modification, propulsion-based delivery, and pharmacological modulation of the TME. Collectively, these approaches offer a promising framework for engineering nanocarrier systems capable of targeted delivery, enhanced tumour penetration, and precise spatiotemporal control of drug release.

1. Introduction

Cancer remains one of the leading threats to human health, with primary treatment modalities including surgery, chemotherapy, and radiotherapy.[1] While surgery and radiotherapy are mainly employed for localised and non-metastatic tumours, chemotherapy is the most commonly used clinical approach when cancer has disseminated systemically.[2,3] Consequently, chemotherapy serves as a crucial strategy to control tumour progression before and after surgical and radiotherapeutic interventions.[4,5] However, conventional chemotherapy not only eradicates cancer cells but also significantly impairs normal cell function.[6] Moreover, small-molecule chemotherapeutic agents typically exhibit short half-lives *in vivo* and are rapidly cleared from the bloodstream, necessitating high-dose administrations that lead to severe systemic toxicity and substantially limit their clinical applications.[7–9]

To address these challenges, the development of nanomedicine-based drug delivery systems (NDDSs) has emerged as a promising solution. Nanocarriers can simultaneously deliver multiple therapeutic agents, offering superior treatment efficacy compared to repeated administrations of free small-molecule drugs.[10,11]

Tumour targeting strategies in NDDSs rely primarily on passive and active mechanisms. Passive targeting exploits the enhanced permeability and retention (EPR) effect, where nanocarriers preferentially accumulate in tumour tissues due to leaky vasculature and poor lymphatic drainage.[12,13] Active targeting is achieved by modifying the nanocarrier's surface with ligands or stimuli-responsive elements that selectively bind to tumour-specific receptors, facilitating enhanced tumour accumulation and controlled drug release.[13] These targeting strategies collectively improve drug concentration at tumour sites while minimising systemic exposure.[14]

Despite these advantages, the clinical application of NDDSs remains challenging.[15] Solid tumours comprise a complex microenvironment consisting of cancer cells, tumour vasculature, extracellular matrix, and metabolic byproducts.[16,17] Although NDDSs employing passive or active targeting strategies have demonstrated prolonged circulation and effective tumour accumulation, their therapeutic efficacy remains restricted by the limited penetration of nanoparticles (NPs) into the tumour core.[18–20] The physicochemical properties of NPs – such as size, shape, surface functional groups, and stimuli-responsive transformations – are key factors influencing tumour accumulation and intratumorally penetration.[21,22]

Addressing the challenge of deep tumour penetration has become a major research focus. Strategies including size-transformable nanoparticles and nanocarriers functionalised with tumour-specific recognition elements have been proposed to enhance tissue infiltration.[23,24] Among these, charge-reversal nanoparticles have emerged as a promising approach.[25] Neutral or negatively charged liposomal NPs benefit from extended circulation and tumour accumulation but often

Australian Institute for Bioengineering and Nanotechnology, The University of Queensland, Brisbane, Queensland 4072, Australia. E-mail: v.bobrin@uq.edu.au

exhibit limited penetration.[26] Conversely, positively charged NPs interact more efficiently with negatively charged cell membranes, improving penetration but suffering from higher cytotoxicity and rapid clearance.[27] Charge-reversal NPs leverage the tumour microenvironment's unique characteristics, such as acidity[28] or redox conditions,[29] to dynamically switch surface charge from neutral/negative during circulation to positive within tumours. This transformation enables enhanced tissue infiltration, cellular internalisation, and therapeutic efficacy, while minimising off-target toxicity.[30]

This review focuses on nanocarrier-based drug delivery systems, providing an overview of different types of nanocarriers (Table 1) and analysing current strategies for enhancing tumour penetration. While various approaches, such as size-transformable nanoparticles and ligand-functionalised carriers, have shown promise in improving tumour targeting and accumulation, significant challenges remain in achieving deep tumour infiltration without compromising systemic circulation time or increasing toxicity. Among these strategies, charge-reversal nanocarrier designs have emerged as a particularly compelling solution. By dynamically modulating surface charge in response to the tumour microenvironment, these systems uniquely address the long-standing trade-off between prolonged circulation and efficient tissue penetration. Accordingly, this review places a special emphasis on charge-reversal nanocarriers, discussing the most extensively studied designs and offering insights into future advancements in this domain.

1.1 Types of nanocarriers

1.1.1 Liposomes. Liposomes, due to their structural similarity to the phospholipid bilayer of cell membranes, can easily fuse with cell membranes, penetrate cellular barriers, and possess good biocompatibility and stability, making them ideal carriers for drug delivery.[99] As an essential drug delivery

Table 1 Advantages and limitations of the five different nanocarriers[a]

Category[b]	Materials/structure	Advantages	Disadvantages	Main forms	Ref.
Lipid-based nanoparticles	Liposomes, solid lipid nanoparticles, nanostructured lipid carriers[31]	Biocompatible, encapsulate both hydrophilic and hydrophobic drugs, modifiable for targeting	Relatively low stability, rapid clearance by the reticuloendothelial system		31–42
Polymeric nanoparticles	Core–shell polymeric nanoparticles,[43] polymeric micelles,[44] nanocapsules	Controlled release, tuneable size, good biodegradability	Complex preparation, possible toxicity of some polymers	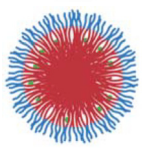	45–59
Inorganic nanoparticles	Gold nanoparticles,[60] mesoporous silica,[61] metal–organic frameworks[62]	Theragnostic potential (therapy + imaging), physical stability, versatile surface modification	Poor biodegradability, uncertain long-term safety	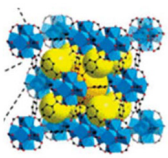	63–71
Biomacromolecule-based carriers	Albumin,[72] gelatin, silk fibroin, DNA origami[73]	Biocompatible, biodegradable, strong targeting ability	Complex structure, high production cost		74–83
Hydrogels	Nanogels,[84] injectable hydrogels,[85] multi stimuli-responsive hydrogels, self-healing hydrogels[86]	Combine advantages of multiple systems, high versatility	Complex fabrication, challenging batch-to-batch consistency	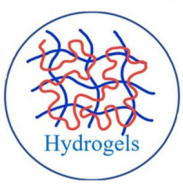	87–94

The images in the table are sourced from top to bottom as follows: adapted with permission ref. 32. Copyright 2021 American Chemical Society; adapted with permission ref. 45. Copyright 2024 American Chemical Society; adapted with permission ref. 63. Copyright 2019 American Chemical Society; adapted with permission ref. 74. Copyright 2024 Elsevier; adapted with permission ref. 87. Copyright 2023 MDPI. [a] Comparative performance data (in clinical perspective) across lipid-based, polymeric, inorganic, and biomacromolecule-based nanocarriers is not discussed in this review; instead, readers are referred to several comprehensive reviews that specifically address this topic.[95,96] [b] While this review focuses on polymer-based and polymer-hybrid nanocarriers, readers interested in extracellular vesicles as drug delivery systems for tumour targeting and penetration are referred to recent comprehensive reviews dedicated to this topic.[97,98]

carrier, liposomes exhibit multiple advantages, such as high drug-loading capacity, robust biological stability, and tuneable drug release kinetics – achieved through their inherent tendency to fuse and reduce surface tension,[100] enabling sustained and controlled drug delivery.[101] Furthermore, their superior biocompatibility and favourable pharmacokinetic profiles – demonstrated *in vivo* by enhanced biodistribution compared to conventional carriers – further support their potential for clinical applications.[102,103] Notably, the exceptional biosafety of liposomes has propelled their integration into advanced nanomedicine delivery systems, driving widespread exploration in both diagnostic and therapeutic applications.

However, liposomes also have certain limitations. For instance, serum proteins can interact with unmodified liposome surfaces, leading to recognition and clearance by macrophages, which significantly hinders efficient drug delivery and reduces circulation time in the bloodstream.[104,105] To overcome these challenges, researchers proposed surface modification strategies for liposomes in the late 1980s and early 1990s. One widely adopted approach involves coating traditional liposomes with inert polymers to enhance their stability. Polyethylene glycol (PEG) is currently the most used polymer for liposome stabilisation. PEGylation reduces the fusion rate between liposomes, thereby improving their stability and prolonging circulation time *in vivo*.[106] Despite the enhanced stability conferred by PEG functionalisation, PEGylated liposomes still lack precise disease-targeting ability and do not offer completely spatiotemporally controlled drug release. To address these limitations, researchers have explored various engineering strategies to further optimise liposome surfaces and their structural composition. For example, conjugating tumour-specific ligands to the liposome surface can endow them with active tumour-targeting capabilities, thereby improving their therapeutic efficacy.[107]

To enhance the efficiency and specificity of drug delivery, liposomal formulations can be systematically engineered into six distinct categories: (i) conventional liposomes, incorporating cholesterol to modulate membrane fluidity and stability;[108,109] (ii) charged liposomes (cationic or anionic) to facilitate cellular uptake or transdermal transport;[110,111] (iii) stealth liposomes, typically modified with PEG to evade immune recognition and prolong systemic circulation;[112,113] (iv) actively targeted liposomes, functionalised with ligands to enable site-specific accumulation *via* receptor-mediated interactions;[114,115] (v) stimuli-responsive liposomes, designed to release their payload in response to specific environmental triggers;[116,117] and (vi) bubble-type liposomes, which encapsulate gas and allow for ultrasound-mediated drug release.[118]

As an example, Wang *et al.* developed a reactive oxygen species (ROS)-responsive polymer vesicle nanosystem with a cascade response combining photodynamic and chemodynamic therapy. Upon laser irradiation, the system generates ROS *in situ* to trigger precise drug release, while a Fenton-like reaction regenerates ROS, overcoming oxygen limitations in the tumour microenvironment. This dual action enhances the efficacy of combined chemotherapy and photodynamic therapy while minimising ROS depletion (Fig. 1).[119]

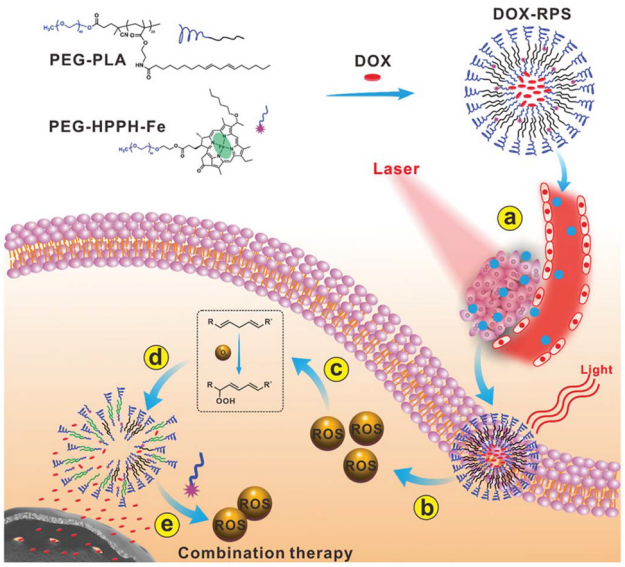

Fig. 1 The schematic illustration of drugs co-delivery strategy to realise chemo-PDT combination therapy. (A) DOX-loaded ROS-responsive polymersomes (DOX-RPS) first passively accumulate in tumour tissue. (B) Upon laser irradiation, HPPH generates reactive ROS *via* a photodynamic process. (C, D) The ROS then oxidise linoleic acid to LAP, which induces structural changes in the polymersome and triggers doxorubicin release. (E) In the presence of HPPH-Fe, ROS are regenerated through a Fenton-like reaction, enabling sustained ROS production and enhancing the combined therapeutic effect. Adapted with permission ref. 119. Copyright 2021 John Wiley & Sons.

1.1.2 Polymeric nanocarriers. Amphiphilic NPs typically consist of a hydrophilic shell and a hydrophobic core, forming a core–shell nanostructure by the self-assembly of amphiphilic polymers and hydrophobic NPs with hydrophilic surface coatings. These core–shell structured NPs are widely recognised for their ability to improve drug loading capacity and transport efficiency. With the continuous advancement of drug delivery systems, the application of polymeric nanoparticles has evolved from the use of early natural polymers (*e.g.*, chitosan and gelatin) and non-biodegradable synthetic materials (*e.g.*, poly(methyl methacrylate) and polystyrene), to the incorporation of biodegradable synthetic polymers (*e.g.*, polylactic acid and poly(lactic-*co*-glycolic acid)) and stimuli-responsive,[120] self-degradable polymers.[121] This transition reflects a growing demand to mitigate the limitations associated with earlier materials, including chronic toxicity, inflammatory responses, and residual accumulation, while simultaneously enhancing biocompatibility and enabling controlled drug release.[122] Beyond serving merely as carriers for the co-delivery of therapeutic agents,[123] the physicochemical properties of polymeric materials can be precisely engineered to modulate their *in vivo* behaviour. This tuneability enables the design of polymers with defined characteristics, such as size, shape, surface charge, and functional groups, tailored to specific therapeutic

requirements.[50] For instance, surface functionalisation can enhance receptor-mediated interactions with target cells, facilitating active targeting. Furthermore, polymers can be engineered to respond to specific physiological stimuli, enabling controlled and site-specific drug release. This level of adaptability supports the development of highly customised drug delivery systems, thereby improving therapeutic efficacy while minimising off-target effects and systemic toxicity.[48,124]

Over the past few decades, a variety of stimuli-responsive NDDSs have been developed to exploit specific characteristics of the tumour microenvironment, including pH gradients,[125] redox potential,[126] and enzymatic activity.[127]

A well-known example is the development of pH-sensitive drug delivery systems, which exploit the pH difference between tumour and normal tissues. These systems are engineered to release therapeutic agents selectively within the acidic tumour microenvironment, thereby enhancing targeting precision and reducing off-target effects on healthy tissues.[128] For instance, poly(β-amino ester) (PBAE) – a pH-sensitive polymer synthesised *via* Michael addition reactions – undergoes hydrolytic degradation under acidic conditions, leading to nanoparticle disassembly and efficient drug release within the tumour microenvironment.[129] Based on this, Lin *et al.* designed a novel pH-sensitive triblock copolymer, methyl polyethylene glycol ether-*b*-poly(β-amino ester)-*b*-polylactic acid (MPEG-*b*-PBAE-*b*-PLA), and investigated the self-assembly of micelles, their microstructure under different pH conditions, and the distribution of doxorubicin (DOX) using dissipative particle dynamics simulations in conjunction with experimental techniques (Fig. 2).

1.1.3 Metal–organic frameworks & inorganic porous nanoparticles. Metal–organic frameworks (MOFs) are a class of crystalline coordination compounds composed of metal ions or clusters bridged by organic ligands, resulting in highly porous, tuneable network structures.[131] Owing to their unique physicochemical properties, MOFs have attracted considerable attention in biomedical research. Notably, their high surface area and pore volume enable exceptional drug-loading capacities, achieved through either *in situ* encapsulation or post-synthetic modification strategies, thereby facilitating controlled and sustained drug release.[132]

Wang *et al.*[133] reported the development of a DNA-templated metal–organic framework nanosphere synthesised *via* a biomineralisation process. This nanostructure enhances the efficacy of chemodynamic therapy by elevating intracellular hydrogen peroxide levels through an *in vivo* cascade reaction (Fig. 3). In addition to MOFs, porous inorganic nanostructures composed of non-metallic materials – such as silica, calcium carbonate, and calcium phosphate – exhibit comparable advantages, including tuneable size, high surface area, and excellent physicochemical stability.[134,135] These materials have been widely utilised as drug carriers in various cancer therapies, such as gene therapy, chemotherapy, and photodynamic therapy. However, the long-term nonspecific accumulation of inorganic nanomaterials in healthy tissues raises concerns regarding potential toxicity, thereby limiting their clinical translation.[136] Consequently, the development of biodegradable inorganic nanomaterials represents a critical direction in biomedical research.[137]

1.1.4 Biomacromolecule-based carriers. Owing to their intrinsic biochemical and biophysical properties, natural biomacromolecules have attracted increasing attention as carriers in biomedical applications in recent years.[75] Their primary advantages stem from their natural abundance, as they can be readily extracted from animal and plant sources, rendering them renewable and sustainable resources. In addition, biomacromolecules exhibit excellent biocompatibility, low immunogenicity, and are enzymatically degradable *in vivo*, yielding metabolites with minimal toxicity.[134] Currently, they are extensively employed across various biomedical platforms, including prodrugs, drug conjugates,[138] nanoparticles,[139] micro-

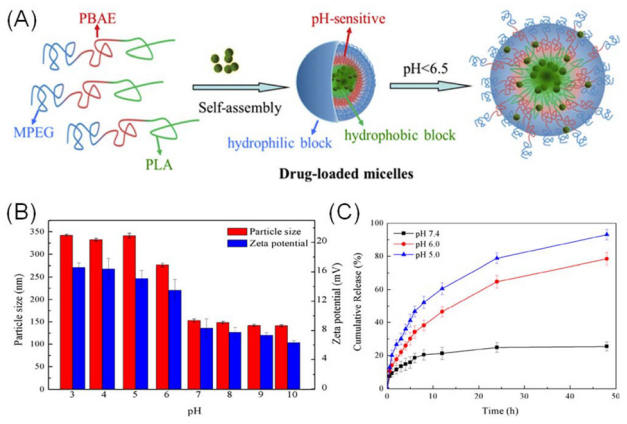

Fig. 2 (A) Schematic illustration of pH-sensitive drug-loaded micelles formed by MPEG-*b*-PBAE-*b*-PLA copolymers. (B) Particle size and zeta potential of micelles at different pH values. (C) Cumulative drug release at pH 7.4, 6, and 5. Adapted with permission ref. 130. Copyright 2018 Elsevier.

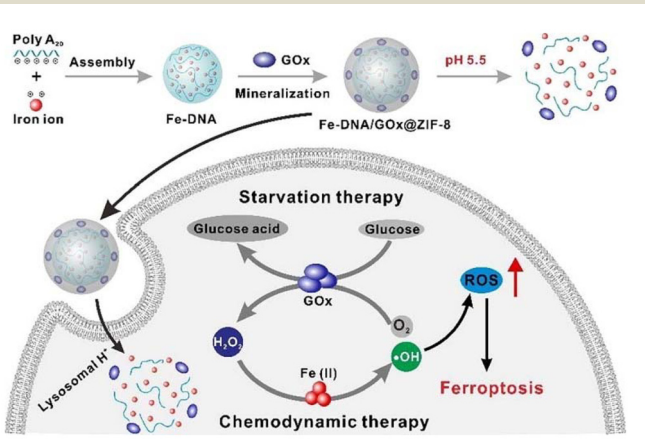

Fig. 3 The MOF nanoparticles formed assembly *via* the coordination of DNA and metal Fe^{2+} ions. Adapted with permission ref. 133. Copyright 2021 Elsevier.

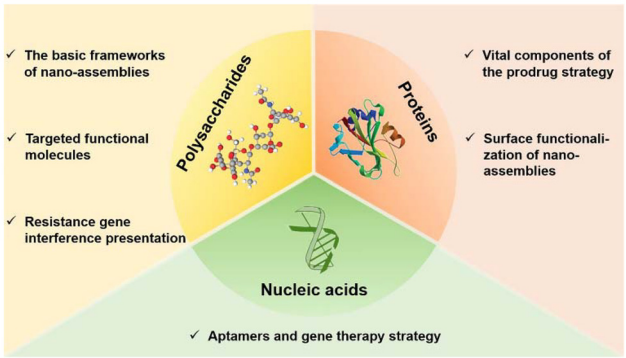

Fig. 4 Representative biomacromolecular components for drug delivery. Adapted with permission ref. 139. Copyright 2021 John Wiley & Sons.

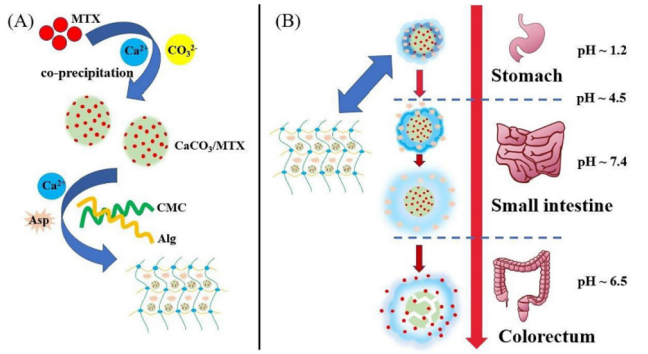

Fig. 6 (A) Schematic illustration of the preparation of methotrexate (MTX)-loaded calcium carbonate ($CaCO_3$) nanoparticles. (B) The nanocomposite particles remain stable in the acidic gastric environment (pH ~1.2), begin to swell and release MTX in the small intestine (pH ~7.4), and ultimately achieve targeted drug release in the colorectum (pH ~6.5). Adapted with permission ref. 151. Copyright 2021 Elsevier.

capsules, hydrogels,[140] and tissue engineering scaffolds (Fig. 4).[141]

Biomacromolecules used as drug carriers have demonstrated the ability to significantly enhance the pharmacokinetic profiles of encapsulated therapeutics, thereby reducing systemic toxicity and immunogenicity. Additionally, their molecular architectures typically feature reactive functional groups – such as hydroxyl, amine, and carboxyl moieties – that allow for further chemical modification, making them highly versatile platforms for the development of NDDSs.[142] However, drug–protein interactions are often nonspecific, with a lack of defined binding sites. Moreover, these sites are susceptible to competitive displacement by endogenous hydrophobic molecules under physiological conditions, which can compromise drug loading efficiency. Notably, apohemoglobin and oxyhemoglobin, both derived from heme-free hemoglobin, provide more selective and stable drug-binding domains due to their well-defined and constrained structural conformations (Fig. 5).

1.1.5 Hydrogels. Hydrogels (HGs) are highly stable, crosslinked polymeric networks, and can be composed of a single polymer (homopolymeric HGs) or a combination of two or more polymers (copolymeric HGs), with the potential to incorporate additional components within the polymeric matrix. Owing to their remarkable water retention capacity, mild fabrication conditions, and excellent biocompatibility, HGs have been extensively utilised as drug delivery carriers for a wide range of therapeutic agents.[144,145] To further enhance their functionality, stimuli-responsive elements or reactive chemical linkages can be integrated into the hydrogel matrix, enabling precise, controlled drug release in response to specific environmental cues.[146] Similar to NPs, certain stimuli-responsive HGs can be formulated as injectable hydrogels, allowing for minimally invasive administration.[147] Beyond drug delivery, HGs exhibit broad applicability in tumour-targeted nanodrug delivery systems, chemical and biosensing platforms,[148] and the development of biomimetic materials.[149]

The chemical structure, composition, biodegradability, biofunctionality, and physicochemical properties (such as mechanical performance, rheology, thermosensitivity, and pH stability) of HGs can be precisely tailored to meet specific requirements. These modifications not only influence the physicochemical characteristics of HGs but also affect drug loading efficiency and release kinetics.[150] For instance, Sheng *et al.* developed a dual-drug delivery system wherein calcium carbonate nanoparticles, co-loaded with methotrexate (MTX) and aspirin (Asp), were encapsulated within HGs composed of alginate (Alg) and sodium carboxymethyl cellulose (CMC), crosslinked by calcium ions (Ca^{2+}). This system effectively shielded MTX from premature metabolism and absorption in the stomach and small intestine, ensuring its therapeutic efficacy at the target site – the colorectal region. Notably, their system exhibited dual pH-responsive drug release behaviour (Fig. 6).[151]

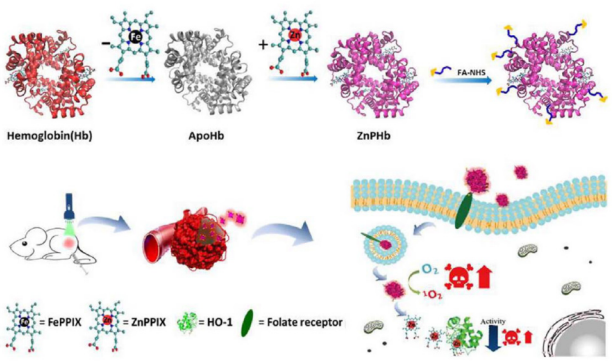

Fig. 5 Hemin (FePPIX)-free hemoglobin carrier with a specific binding site to couple with drugs. Adapted with permission ref. 143. Copyright 2019 Springer Nature.

2. Design of nanocarriers for deep tumour penetration

Recent studies have highlighted the crucial role of the tumour microenvironment (TME) in promoting tumour cell prolifer-

ation, metastasis, and invasion.[152,153] The TME is a highly complex and dynamic system that differs markedly from normal tissue in several key aspects, including its biochemical milieu (*e.g.*, mildly acidic pH of 6.5–6.8 and severe hypoxia), cellular composition (*e.g.*, the presence of tumour-associated macrophages), and the elevated levels of specific bioactive molecules (*e.g.*, glutathione, hydrogen peroxide, and matrix metalloproteinases).[154] These unique characteristics have inspired the development of tumour-targeted nanomedicines, such as TME-responsive nanodrug delivery systems and regulatory agents aimed at modulating or normalising the TME.[155]

Although NPs benefit from the EPR effect, which facilitates greater accumulation at tumour sites compared to small-molecule drugs, the heterogeneity of the TME remains a significant challenge.[156,157] Many NPs – typically around 100 nm in diameter – tend to accumulate near tumour vasculature but exhibit limited penetration into the deeper tumour tissue, thereby reducing therapeutic efficacy.[158] To overcome this limitation, two principal strategies have been proposed. The first involves optimising the physicochemical properties of NPs, such as size, shape, and surface chemistry, all of which critically influence their behaviour within the complex physiological environment. Rational tuning of these parameters can enhance intratumoural distribution and tissue penetration.[159,160] The second strategy focuses on remodelling the TME, including vascular normalisation and extracellular matrix (ECM) modification, to establish a microenvironment more conducive to the effective transport and action of nanomedicines.[161]

During nanoparticle infiltration into tumours, multiple physiological barriers must be overcome, including aberrant vascular architecture, elevated interstitial fluid pressure, abundant stromal cell populations, and a dense ECM network.[162] These factors collectively hinder the effective penetration and uniform distribution of nanodrug delivery systems within tumour tissues, posing substantial challenges for therapeutic efficacy. As a result, overcoming these biological obstacles remains a critical focus in the rational design and development of next-generation nanomedicines for cancer therapy.

2.1 Size-transformable nanoparticles

In nanomedicine, the rational design of size-switchable smart drug delivery systems is essential for the effective transport of nanotherapeutics to tumour sites. NPs in the size range of 100–200 nm typically exhibit prolonged circulation times and preferential accumulation at tumour sites *via* the EPR effect.[163] However, their relatively large size limits deep tumour tissue penetration and hampers cellular uptake in regions distant from the vasculature. In contrast, smaller NPs (<50 nm) demonstrate reduced adhesion to tumour vasculature and extracellular matrix components, thereby enabling improved intratumoural penetration and more uniform drug distribution.[164] This size-dependent paradox has driven the development of NPs engineered to undergo size reduction in response to stimuli within the TME. These smart delivery systems are designed to initially remain above 100 nm, leveraging the EPR effect for efficient accumulation at tumour sites. Upon exposure to specific TME cues, they shrink to sizes below 50 nm, enabling deeper penetration through ECM into the tumour interior.[165,166] Moreover, some advanced designs have combined this size-shrinkage capability with mechanisms targeting the elimination of peripheral tumour cells, thereby synergistically overcoming biological barriers and enhancing nanoparticle transport toward the tumour core.[167] Wang *et al.*[168] developed a tumour-penetrating drug delivery system based on MOFs. In this approach, a newly designed aggregation-induced emission photosensitiser was encapsulated within an iron(III)-based MOF (MIL-100) to form PS@MIL-100. The surface of this composite was subsequently coated with polyethylene glycol methyl ether (PEG) conjugated with Dox at the distal end, yielding Dox-PEG-PS@MIL nanoparticles (NPs) with an initial diameter of approximately 120 nm. Upon accumulation at the tumour site, the elevated hydrogen peroxide (H_2O_2) levels in TME triggered the release of the AIE PS from the MOF structure. Light irradiation then activated photodynamic therapy *via* the aggregation-induced emission photosensitiser, resulting in the partial ablation of peripheral tumour cells. Concurrently, Dox-PEG underwent self-assembly in response to the TME, forming ultra-small Dox NPs capable of deeper tumour penetration. This dual-responsive strategy significantly enhanced intratumoural drug diffusion and therapeutic efficacy (Fig. 7).

2.2 Charge-reversal nanoparticles

DOXIL, the first liposomal nanoparticle formulation approved for clinical use, is surface modified with PEG to confer a 'stealth effect', thereby reducing recognition by the mononuclear phagocyte system and prolonging systemic circulation. This modification enhances the EPR effect, facilitating greater accumulation in tumour tissues.[169] However, despite its effective tumour accumulation, the relatively large particle size and the negatively

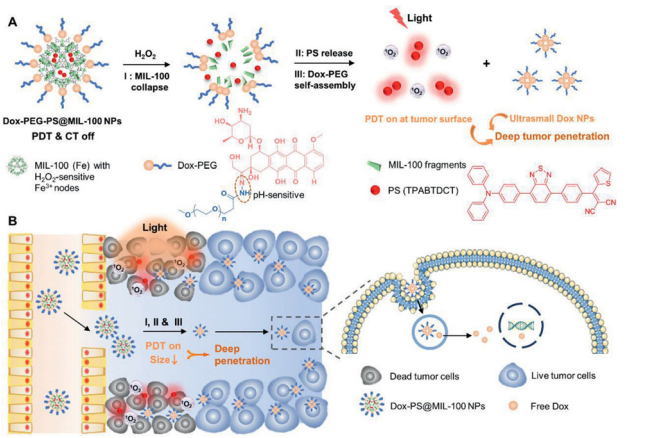

Fig. 7 (A) Based on Fe^{3+}-MOF, Dox-PEG-PS@MIL-100 NPs with dual activation size reduction characteristics were developed to realise deep tumour penetration. (B) Proposed mechanism of deep tumour penetration and therapeutic action. After the size reduction triggered by H_2O_2 and light, the nanoparticles exhibit enhanced tissue penetration. Adapted with permission ref. 168. Copyright 2021 John Wiley & Sons.

charged PEG corona hinder deep tumour penetration and limit cellular uptake by tumour cells, ultimately reducing therapeutic efficacy.[170] Subsequently, V. P. Shastri and colleagues discovered that positively charged NPs exhibited a much higher degree of binding and internalisation by endothelial cells in tumours compared to neutral or negatively charged NPs, primarily due to their electrostatic attraction to the negatively charged tumour cell membranes and extracellular matrix.[171] However, the strong positive surface charge is also associated with increased toxicity and undesirable interactions with healthy tissues.[172] As a result, there has been growing interest in the development of charge-reversal NPs, which maintain a neutral to slightly negative surface charge during circulation but can switch to a positive charge when reaching the tumour site through responsive changes. This design helps resolve the contradiction between the need for prolonged circulation time and enhanced tumour tissue penetration and cellular internalisation efficiency.[173–175]

Wang *et al.*[176] developed a series of polymeric NPs with varying surface charges and studied their performance *in vivo*. Poly(ethylene glycol)-*b*-poly(D,L-lactic acid) (PEG-*b*-PLA) copolymers with different lipid compositions self-assembled into NPs with different surface charges (Fig. 8). The researchers systematically investigated the impact of surface charge on the pharmacokinetics, tumour accumulation, tumour penetration, and therapeutic efficacy of these nanoparticles. Although positively charged nanoparticles showed slightly reduced circulation time and tumour accumulation compared to neutral or negatively charged counterparts, they demonstrated significantly stronger tumour growth inhibition. This superior therapeutic effect was attributed to their enhanced ability to penetrate the tumour extracellular matrix, leading to deeper intratumoural distribution, greater drug accumulation, and ultimately more effective tumour suppression.

Cationic polymers such as poly(L-lysine) (PLL) are highly effective for targeting cell nuclei, making them particularly suitable for the delivery of nucleic acid drugs.[177] However, the strong positive charge of PLL often results in severe toxicity, significantly limiting its clinical application due to potential adverse effects *in vivo*.[178] To address this challenge, Zhou *et al.*[179] designed a PLL precursor polymer capable of charge reversal in acidic environments, thereby mitigating toxicity. The primary amines of PLL were amidated to form β-carboxyamides (PLL-amide), which are unstable under acidic conditions. PLL-amide carries a negative charge, exhibits reduced toxicity, and interacts minimally with cells, making it safer for systemic administration. Upon encountering an acidic microenvironment, such as TME, the acid-sensitive amide bonds undergo hydrolysis, exposing the primary amines and regenerating PLL. The protonated PLL regains a strong positive charge, promoting lysosomal escape and enabling subsequent nuclear entry. To further enhance tumour targeting, folic acid (FA) ligands and the chemotherapeutic drug camptothecin (CPT) were conjugated to the PLL-amide backbone, forming a nuclear-targeted polymer–drug conjugate (FA-PLL-amide-CPT). This conjugate selectively targets cancer cells overexpressing folate receptors and delivers CPT to the cell nucleus. Furthermore, CPT is linked *via* a glutathione-responsive disulfide bond, ensuring efficient drug release in the intracellular environment to maximise therapeutic efficacy (Fig. 9).

2.3 Shape-transforming nanoparticles

Organisms in nature exhibit remarkable morphological diversity, with distinct body plans evolving to meet specific environmental demands and enhance survival. Notable examples include the spherical capsid of the HIV virus, which optimises space for genetic material storage; the cylindrical structure of the tobacco mosaic virus, which facilitates efficient invasion of

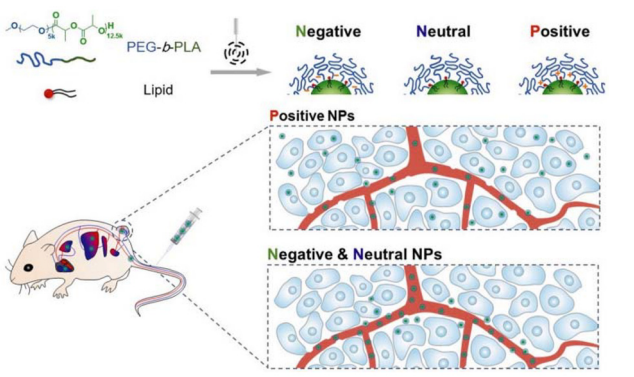

Fig. 8 Cationic PEGylated NPs exhibited significantly enhanced tumour penetration ability compared to their neutral or anionic counterparts across five tumour models. Adapted with permission ref. 176. Copyright 2016 Elsevier.

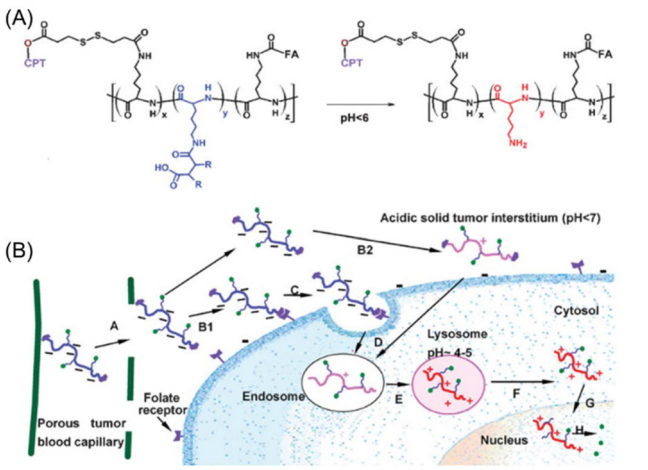

Fig. 9 (A) The design of NPs with charge reversal characteristic triggered by the instability of β-carboxyamide under different pH condition. (B) The conjugate accumulates in the acidic environment of the endosome and lysosome within tumour tissues. The amide bonds hydrolyse, releasing the charge-reversed PLL carrier, which disrupts the lysosomal membrane, escapes into the cytosol, and enters the nucleus to release the drug. Adapted with permission ref. 179. Copyright 2009 John Wiley & Sons.

plant cells; the radially symmetric Stella bacteria, which maximise surface area for nutrient absorption in aquatic environments; and the specialised cellular morphologies found in multicellular organisms, such as discoid erythrocytes for oxygen transport and branched neurons for neural networking, enabling tissue differentiation and functional compartmentalisation.[180,181] Inspired by these biological systems, numerous studies have demonstrated that the shape of NPs critically influences their cellular uptake efficiency, intracellular transport dynamics, and overall transport mechanisms.[182] For instance, spherical NPs tend to accumulate more effectively at tumour sites by exploiting the EPR effect, whereas rod-shaped NPs are generally internalised more efficiently by cells, and fibrous NPs can persist at tumour sites for extended periods, potentially enhancing therapeutic outcomes.[183]

Moreover, NPs with different shapes exhibit distinct tissue penetration capabilities, largely due to their varied interactions with tumour endothelial cells and the dense ECM. For example, experiments utilising *in vitro* three-dimensional (3D) cell spheroid models demonstrated that nanosheets with a diameter of 325 nm and a height of 100 nm achieved superior tissue penetration compared to rod-shaped NPs measuring 100 nm in diameter and 400 nm in length.[184] Similarly, another study showed that CdSe/CdS quantum dot (QD)-based NPs, with dimensions of 15 nm in diameter and 54 nm in length, penetrated more effectively from the perivascular region to the tumour core in an E0771 orthotopic breast cancer model than spherical NPs with a diameter of 35 nm.[185]

As known, cells mainly take up NPs through endocytosis. Particles such as large ellipsoids, are more easily swallowed through phagocytosis process. However, smaller particles are often taken in by the cell through different methods: larger ones through macropinocytosis (larger than 1 μm), medium-sized ones through clathrin-mediated endocytosis (around 120 nm), and smaller ones through caveolae-mediated endocytosis (around 60 nm). Moreover, the shape of NPs plays a crucial role in their uptake.[186] Particles with large or flat surfaces are more easily engulfed, while sharp or highly curved structures may pierce the cell membrane and be internalised directly. Studies have also shown that NPs with at least one very small dimension are more efficiently taken up by cells (Fig. 10).[187]

In addition, the symmetry of nanoparticles can also play a decisive role in modulating their interactions with cell membranes and subsequent uptake pathways. In the study by Monteiro, Gu, Bobrin *et al.*, three distinct PNIPAM-coated nanostructures, *i.e.*, symmetric spheres and rods and asymmetrically structured tadpoles, were prepared using the temperature-directed morphology transformation method[188] and evaluated for uptake by triple-negative breast cancer cells (MDA-MB-231) (Fig. 11A).[189] While all three nanostructures were comparable in size and surface chemistry, their distinct symmetry led to markedly different cellular internalisation efficiencies. Even at a low concentration of 5 μg mL^{-1}, both spherical and tadpole-shaped nanoparticles were internalised by nearly all TNBC (MDA-MB-231) cells (~100% uptake) (Fig. 11B). In contrast, rod-shaped nanoparticles achieved

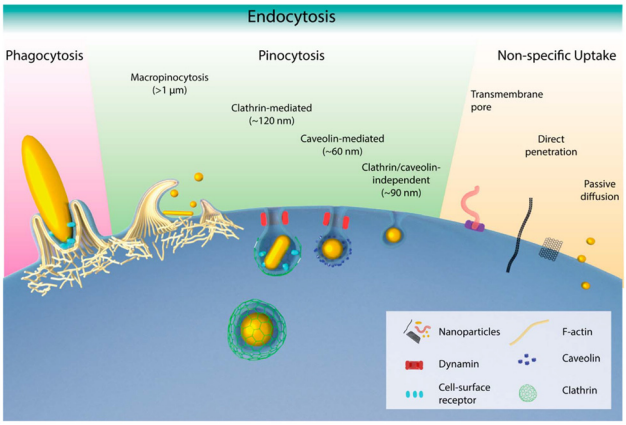

Fig. 10 Schematic representation of different endocytic mechanisms for NPs with varying shape: flat or large-surface particles are easily engulfed, while sharp or highly curved particles may pierce the cell membrane for direct entry. NPs with at least one small dimension tend to be more effectively internalised. Adapted with permission ref. 187. Copyright 2017 American Chemical Society.

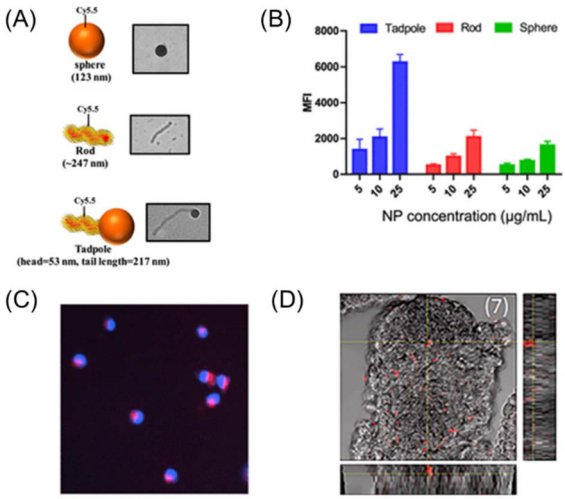

Fig. 11 (A) Symmetric, *i.e.*, spheres and rods, and asymmetric tadpole-shaped nanoparticles conjugated with a Cy 5.5 fluorescent dye. (B) Mean fluorescence intensity measured in cells transfected with nanoscale tadpole-shaped, rod-shaped, and spherical nanoparticles. (C) Fluorescence image showing the intracellular localisation of tadpoles in MDA-MB-231 cells. Adapted with permission ref. 189. Copyright 2020 American Chemical Society. (D) Penetration of RGD-functionalised tadpoles (red dots) into HCT116 spheroids. Adapted with permission ref. 193. Copyright 2024 American Chemical Society.

similar uptake levels only at a higher concentration of 10 μg mL^{-1}. Mean fluorescence intensity (MFI) analysis revealed a near-linear, dose-dependent increase in cellular uptake across all three nanoparticle types. While rods and spheres exhibited comparable uptake levels across the tested doses, tadpole-shaped nanoparticles consistently demonstrated significantly higher transfection efficiency, as reflected by their markedly elevated MFI values. At a concentration of 25 μg mL^{-1}, the

cells contained 20-fold and 10-fold more tadpoles and rods, respectively, compared to spherical nanoparticles. Fluorescence microscopy of TNBC cells showed that the tadpole nanoparticles accumulated in large intracellular compartments (>2 μm) located adjacent to the nucleus (Fig. 11C). Additional mechanistic investigations, including the use of endocytic inhibitors and temperature-dependence assays, confirmed that the internalisation of tadpoles was both rapid and energy-dependent, and predominantly occurred *via* phagocytosis driven by their anisotropic shape and the thermoresponsive PNIPAM corona.[190–192] Tadpole-shaped nanoparticles also demonstrated efficient penetration into tumour spheroids, where they were selectively internalised by spherical cells expressing stem cell markers (Fig. 11D). Moreover, they exhibited a density-dependent influence on the proliferation and maintenance of colon cancer stem cells, modulating both sphere formation and stemness characteristics.[193]

Jia *et al.*[194] designed a NDDS that simultaneously exhibits stimuli-responsive shape transformation and surface charge inversion, enabling the combined application of chemo- and photodynamic therapies. This strategy optimises blood circulation time, tumour permeability, and tumour retention of NPs, ultimately enhancing antitumor efficacy. In this system, the hydrophobic photosensitiser chlorin e6 (Ce6), the hydrophilic chemotherapeutic agent berberine (BBR), and a matrix metalloproteinase-2 (MMP-2)-responsive peptide (PLGVRKLVFF) were conjugated to form a linear triblock copolymer, BBR-PLGVRKLVFF-Ce6 (BPC), which could self-assemble into nanostructures. The positively charged BPC was then complexed with poly(ethylene glycol)-histidine (PEG-His) to form PEG-His@BPC, resulting in nanoparticles with a negative surface charge and prolonged blood circulation time. Upon reaching the acidic tumour microenvironment, protonation of histidine residues led to the detachment of the PEG-His shell, triggering charge inversion and size reduction of PEG-His@BPC. Subsequently, the exposed MMP-2 cleavage sites were enzymatically degraded by the highly expressed MMP-2 in tumours, converting the spherical NPs into nanofibers that released BBR to induce tumour cell apoptosis. Compared to the original spherical structures, the resulting nanofibers containing Ce6 exhibited prolonged retention at the tumour site, thereby enhancing the therapeutic outcome (Fig. 12). Similarly, Gao *et al.* reported a multifunctional nanoplatform (dBET6@CFMPD) for the treatment of breast cancer by co-delivering the PROTAC molecule dBET6 and a photosensitizer (Ce6) within an MMP-2-sensitive nanocarrier, which enables targeted release and *in situ* transfer the shape into nanofibers in the tumor microenvironment.[195,196]

The design strategies of tumour-responsive and deformable drug delivery carriers are comprehensively elaborated in this review.[197]

2.4 Nanoparticle surface modification

In general, during the drug delivery process, the TME serves as the initial and most direct point of interaction for NPs. Consequently, this interaction plays a critical role in determining the penetration efficiency of NPs within solid tumours.[198] Since surface modifications of most NPs can be performed under mild conditions in a relatively straightforward manner, this strategy is considered highly feasible for large-scale production and clinical translation. Therefore, surface modification remains one of the simplest and most effective approaches to promote deep penetration of nanoparticle-based therapeutics into solid tumors.[199–201]

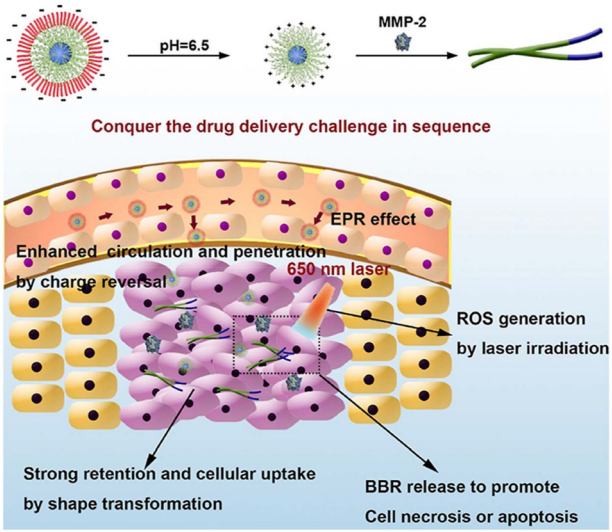

Fig. 12 The design of NPs capable of undergoing charge reversal (from negative to positive) and shape transformation (from spherical to linear) specifically within the tumour microenvironment, thereby improving drug penetration and extending tumour retention time. Adapted with permission ref. 194. Copyright 2022 Elsevier.

To date, a wide range of tumour-targeting ligands, including folic acid, antibodies, zoledronic acid, alendronate, and various peptides, have been employed to specifically target primary and metastatic tumours.[202–204] Among these ligands, the RGD peptide family is one of the most widely used for promoting cellular uptake.[205,206] First discovered by Ruoslahti[207–209] during the screening of tumour metastasis-associated peptides, the RGD peptide is a cyclic nonapeptide with the sequence CRGDKGPDC. When covalently attached to the surface of NPs, the iRGD peptide markedly enhances their tumour penetration capability. The iRGD-mediated enhancement of nanoparticle tumour penetration occurs primarily through a two-step mechanism: (1) specific binding of the iRGD peptide to αv integrins expressed on the tumour endothelium, followed by (2) proteolytic cleavage of the iRGD peptide, exposing a CendR (C-end Rule) motif, which subsequently binds to neuropilin-1 receptors, thereby promoting deeper nanoparticle penetration into the tumour tissue.[210,211]

Based on extensive research into the surface modification of NPs, a variety of strategies have been developed and applied.[193,212] For instance, Li *et al.*[213] synthesised a poly(ethylene oxide)-*b*-poly(ε-caprolactone) (PEO-*b*-PCL) block copolymer and modified the PCL block with lipoic acid and the PEO block with hydrazide, amine, or azide groups. The resulting

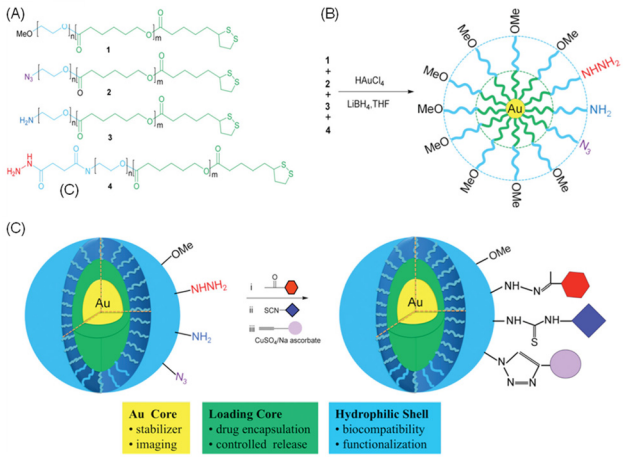

Fig. 13 (A) Block copolymers are designed with a thioic acid group at the hydrophobic PCL end to bind gold, and a functional group at the hydrophilic PEO end for further modification. (B) The polymers are grafted on the surface of Au NPs. (C) In water, the nanoparticles have a gold core (yellow); a hydrophobic PCL layer (green) for loading hydrophobic drugs; and a biocompatible PEO shell (blue). Adapted with permission ref. 213. Copyright 2011 American Chemical Society.

polymer can be utilised to fabricate NPs with surface-modifiable groups. These NPs consist of a gold nanoparticle core, a PCL layer for drug loading, a biocompatible hydrophilic PEO segment, and three different reactive groups that enable further surface functionalisation. Through click chemistry reactions, these NPs can efficiently react with structures containing ketone, isocyanate, or alkyne functional groups (Fig. 13). This functionalisation allows modification with various components, such as cell-penetrating peptides to enhance cellular uptake, histidine-rich peptides to facilitate lysosomal escape, and fluorescent labels for quantification.

Emerging trends in this field include the use of cell membrane-coated nanoparticles (CM-NPs) for targeting TME. These nanoparticles are designed to mimic the properties of their source cells, such as red blood cells, cancer cells, macrophages, and even hybrid combinations of multiple cell types.[214–216] By leveraging these natural membranes, CM-NPs can evade immune surveillance, extend their circulation time in the bloodstream, and achieve homotypic targeting of tumour tissues with high specificity. For example, Fang, Zhang *et al.* demonstrated cancer cell membrane-coated nanoparticles for both anticancer vaccination and targeted drug delivery.[217] The membrane derived from murine B16-F10 melanoma cells was used to coat biodegradable polymeric nanoparticles. This coating endowed the nanoparticles with a range of cancer cell-associated surface antigens and adhesion molecules, enabling them to closely mimic tumour cells. As a result, these CCNPs exhibited strong homotypic targeting ability, meaning they preferentially accumulated in tumours of the same origin due to membrane-mediated recognition and adhesion. This targeting significantly enhanced the accumulation of nanoparticles at the tumour site and improved therapeutic efficacy.

2.5 Gas-driven nanoparticles

Gas-driven nanoparticles represent an emerging strategy for controlled drug release, leveraging gas generation to trigger the release process. Ammonium bicarbonate (NH_4HCO_3), a commonly used agent, produces carbon dioxide and ammonia under specific conditions. Both gases are normal metabolic byproducts that can be safely eliminated from the body. As a result, NH_4HCO_3 can be encapsulated within nanocarriers such as liposomes or poly(lactic-*co*-glycolic acid) (PLGA). Upon gas release, internal pressure is generated, which helps disrupt dense tumour tissue and create temporary openings. These openings facilitate deeper penetration of NPs into the tumour, thereby enhancing drug delivery and improving therapeutic efficacy. This mechanism offers a promising approach for precise and efficient drug delivery.[218,219]

Li *et al.*[160] developed a carrier-free "nanobomb" with a polydopamine (PDA) coating for on-demand drug release at specific sites. Initially, the hydrophobic chemotherapy drug doxorubicin (Dox) self-assembled into nanoparticles (DNPs), which were then coated with PDA due to its ability to self-polymerise and form a thin layer in alkaline solutions (pH = 8.5). The DNPs were combined with ammonium bicarbonate to form the DNPs/N@PDA system. The PDA coating prevented premature drug leakage during circulation, allowing for enhanced drug accumulation at the tumour site *via* the EPR effect. Upon reaching the tumour, DNPs/N@PDA underwent rapid expansion and rupture upon exposure to near-infrared (NIR) light. The thermal decomposition of NH_4HCO_3 generated carbon dioxide and ammonia, triggering a "bomb-like" release of Dox. This release mechanism was facilitated by the strong NIR absorption and high photothermal conversion efficiency (up to 40%) of the PDA membrane (Fig. 14).

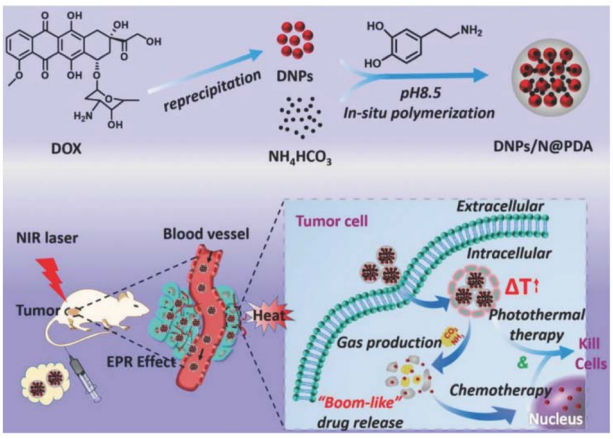

Fig. 14 A schematic illustration of the formation of nanoparticles by dopamine self-polymerisation under alkaline conditions to encapsulate Dox NPs and NH_4HCO_3. Upon NIR irradiation, the polydopamine shell converts light into heat, causing thermal decomposition of NH_4HCO_3 and rapid generation of CO_2. This gas production drives nanoparticle movement and enables burst-like drug release. Adapted with permission ref. 160. Copyright 2018 John Wiley & Sons.

Researchers have also developed micro-/nanorobots that utilise gas release as a driving force for self-propulsion, offering enhanced tumour tissue penetration. For example, Zhou *et al.*[220] designed a NIR light/gas dual-driven calcium carbonate microrobot (JCPMs) that exhibits NIR-induced thermophoresis in blood-mimicking media and self-driving propulsion *via* CO_2 bubble generation in the acidic TME. These two driving forces enable JCPMs to overcome multiple biological barriers during drug delivery. Initially, the thermophoretic motion of JCPMs facilitates deep penetration within the tumour. Subsequently, after internalisation by tumour cells, CO_2 gas-driven propulsion enhances lysosomal escape, allowing for precise intracellular drug release.

Furthermore, nitric oxide (NO) gas has been shown to effectively promote the degradation of collagen in the tumour ECM and inhibit multidrug resistance associated with cancer chemotherapy. Due to its high affinity for oxygenated hemoglobin, NO is rapidly cleared from the body upon binding to oxygenated hemoglobin, limiting its duration of action in systemic circulation.[221,222] Based on this, Wan *et al.*[223] developed a cage-like nanocarrier, HFLA-DOX, designed to actively target cancer cells. The nanocarrier utilises folic acid (FA) as a targeting agent, loading both L-arginine and the anticancer drug doxorubicin (Dox). The FA component enables specific binding to folate receptors, which are overexpressed on cancer cells, thereby facilitating targeted delivery to the tumour. L-Arginine, which can form hydrogen bonds with the cell membrane, enhances the internalisation efficiency of HFLA-DOX by tumour cells. Due to the elevated levels of nitric oxide synthase and reactive oxygen species in TME, L-arginine within HFLA-DOX decomposes to generate NO gas. This triggers the self-propulsion of the nanocarrier, aiding its transport within the tumour and enhancing distribution across various cellular compartments.

2.6 Magnetically driven nanoparticles

To enhance the performance of NPs, researchers have explored various strategies, such as size or surface charge-responsive NPs, to improve tissue penetration. However, these approaches often encounter limitations in *in vivo* applications, as they are highly sensitive to minor fluctuations in the TME. To overcome these challenges, micro/nano motors, a novel class of drug delivery carriers, have garnered significant attention. These systems convert external stimuli – such as magnetic fields, ultrasound, or light – or environmental changes within the TME into mechanical forces. This transformation provides NPs with self-propulsion, significantly enhancing their ability to penetrate tissues and improve therapeutic delivery.[224–226]

Early applications of magnetic nanotechnology in biomedicine have encompassed a range of areas, including cell labelling, laboratory analysis, synthetic magnetic separation techniques, imaging, magnetic drug targeting, hyperthermia, and disease diagnosis using externally driven nanoparticles (MNPs).[227,228] For example, magnetic nanofibers have been shown to exhibit self-propulsion under the influence of strong magnetic fields when placed in untreated human serum samples. Additionally, helical micro/nano structures can efficiently navigate through hyaluronic acid solutions – commonly found in biological tissue gaps – when driven by a rotating magnetic field.[229]

Shao *et al.*[230] developed a multifunctional composite nanocarrier (M-MSNs-DOX), consisting of an iron oxide (Fe_3O_4) magnetic core and mesoporous silica (SiO_2) loaded with Dox. M-MSNs-DOX exhibit a small size, tuneable aspect ratio, porous structure, and superior magnetically driven performance. When exposed to an external magnetic field, M-MSNs-DOX are efficiently internalised by tumour cells, where they release Dox in response to specific stimuli. Experimental results demonstrate that M-MSNs-DOX significantly inhibit tumour growth in both subcutaneous and liver orthotopic tumour mouse models, while minimising systemic toxicity (Fig. 15).

Similarly, Zhu *et al.*[231] developed a polymeric drug delivery system named DAT-PPED&F, with an approximate size of 180 nm. This system comprises a polyphosphate core, magnetic iron nanocubes, and a tumour extracellular pH-responsive transactivator (TAT). The study demonstrated that, when driven by an external magnetic field, DAT-PPED&F exhibited superior tumour tissue penetration. *In vivo*, DAT-PPED&F efficiently delivered Dox to nearly all tumour cells, resulting in remarkable therapeutic efficacy against tumours.

2.7 Microbial-driven nanoparticles

The field of drug delivery has recently faced growing demands to develop propulsion mechanisms that enable targeted delivery of therapeutic and diagnostic agents to specific disease sites within the body. One such propulsion structure com-

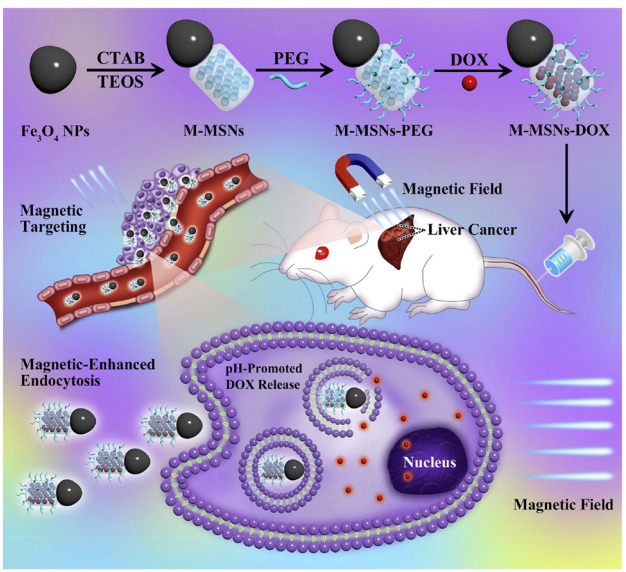

Fig. 15 Schematic illustration of Janus "nano-bullet" multifunctional NPs (M-MSNs-DOX) integrate a magnetic Fe_3O_4 head and a DOX-loaded mesoporous SiO_2 body, enabling magnetically enhanced endocytosis and pH-responsive drug release. Adapted with permission ref. 230. Copyright 2016 Elsevier.

monly found in the microscopic world is the flagellum, which is present in bacteria and sperm cells.[184,232] The powerful self-propulsion of flagella can be harnessed as a driving mechanism in drug delivery, enabling active drug administration. Research has demonstrated that sperm cells can function as propulsion devices for NPs. By physically or chemically loading NPs onto sperm, a novel NP structure can "swim" through the complex human environment, utilising biological self-propulsion instead of relying solely on passive blood circulation.[233] Using sperm-driven propulsion, micro/nanoscale drug carriers loaded with anticancer drugs can be actively transported to tumour sites, facilitating more effective drug accumulation and enhanced therapeutic outcomes. Building on this concept, Zhang *et al.*[234] developed artificial magnetic flagella that are driven by rotating or oscillating magnetic fields. Similarly, Travis *et al.*,[235] inspired by the propulsion mechanisms of biological sperm cells, reconstructed molecular motors to design self-propelled nanorobots.[236]

Moreno *et al.* reported the use of facultative anaerobic *Escherichia coli* (*E. coli*) as a carrier for transporting mesoporous SiO_2 nanoparticles (MSNs) loaded with the chemotherapy drug Dox to tumour sites (Fig. 16).[237] The bacterial wall was functionalised with azide-modified amino acids (azido-D-alanine), which bind to the bacterial surface through standard bacterial metabolic processes. A subsequent click chemistry reaction, utilising the well-established azide–alkyne cycloaddition, covalently linked the *E. coli* to the MSN. The bacteria then utilised their inherent motility to propel the MSNs into the core of a 3D tumour model, which featured a high-density extracellular matrix. This approach offers significant advantages over non-functional NPs by demonstrating the potential of non-pathogenic bacteria as drug carriers for solid tumour treatment. Additionally, the use of microorganisms capable of adapting to the hypoxic or acidic tumour microenvironment enhances nanoparticle penetration and distribution within malignant tissues.

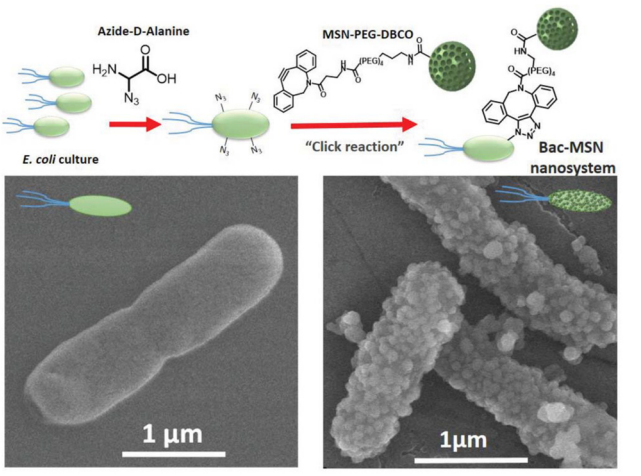

Fig. 16 Schematic illustration of engineered *E. coli* as active carriers for doxorubicin-loaded mesoporous silica nanoparticles (MSNs) by bioorthogonal azide–alkyne click chemistry. Adapted with permission ref. 237. Copyright 2020 John Wiley & Sons.

The aforementioned gas-propelled, magnetically actuated,[238] and microorganism-driven drug delivery platforms[239,240] can be collectively categorised as externally actuated drug delivery systems, and are discussed in greater detail in this review article.[241]

2.8 Pharmacological regulation of tumour microenvironment

ECM primarily consists of substances such as collagen, fibronectin, hyaluronic acid, and glycoproteins.[242] However, the increased fibrosis in tumour tissues significantly hampers the penetration of macromolecular drugs into the tumour. Consequently, therapeutic agents that inhibit ECM fibrosis can enhance the tumour penetration of NPs.[243,244] Jain *et al.*[245] were the first to investigate the use of losartan in tumour therapy. Losartan, an angiotensin II receptor antagonist, also exhibits anti-fibrotic properties by targeting endothelial cells. Treatment with losartan has been shown to reduce the level of type I collagen in various tumour models.[246] In a study involving mice bearing human Mu89 melanoma, pretreatment with losartan significantly improved the infiltration of 100 nm polystyrene NPs from blood vessels into the tumour core, compared to control mice that did not receive losartan. Subsequent histological analysis confirmed that losartan disrupted collagen fibres within the tumour tissue, thereby facilitating deeper nanoparticle penetration into the tumour microenvironment.[247]

In addition, certain enzymes have been utilised to remodel the ECM. For instance, a study demonstrated that NPs functionalised with collagenase penetrated the tumour core at significantly higher levels – approximately four times greater – compared to their non-collagenase-modified counterparts.[248] Similarly, bromelain, a protease from the papain family, can degrade protein components in the ECM.[249] When coupled with SiO_2 NPs, bromelain was found to double the penetration depth of SiO_2 NPs within tumour tissue (from 500 to 1000 μm) and significantly enhance the distribution of NPs in mouse breast cancer (4T1) tumours following tail vein injection.[250]

Moreover, the localised hyperthermia induced by photothermal therapy can also effectively remodel the tumour microenvironment, thereby facilitating the deep penetration of nanotherapeutics into tumour tissues.[251]

2.9 Thermal effects to promote deep tumour penetration of nanoparticles

Hyperthermia and thermosensitive drug delivery systems have been employed to enhance the penetration of nanoparticles NPs into tumours.[252] Mild hyperthermia has been shown to induce inter-endothelial gaps of approximately 10 μm, which facilitate the deeper penetration of NPs into the tumour core.[253] For example, researchers developed a thermosensitive liposome-based drug delivery system for doxorubicin (DOX-TSL) in combination with local hyperthermia therapy.[254] They studied its impact on the efficiency of DOX-TSL internalisation by cells and its tissue penetration capability in both 2D and 3D human ovarian cancer cell models. The results demon-

strated that DOX-TSL exhibited superior tissue penetration compared to conventional NPs. *In vitro* experiments showed that, under high-intensity focused ultrasound, DOX-TSL was able to rapidly release its payload. *In vivo*, following hyperthermic stimulation *via* high-intensity focused ultrasound, DOX-TSL effectively overcame biological barriers and rapidly penetrated the tumour core. Mice treated with high-intensity focused ultrasound displayed a tumour inhibition rate of 65.2%, highlighting that hyperthermia significantly enhanced both intratumoural penetration and the anticancer efficacy of DOX-TSL.[255]

3. Charge-reversal nanoparticle design strategies

As discussed above, one of the major challenges in cancer nanomedicine is the limited accumulation of therapeutic agents within the tumour core and inside tumour cells. Following intravenous injection, NPs must navigate a series of biological barriers.[256] Initially, NPs are transported through the bloodstream to the tumour site. Subsequently, they must extravasate from the vasculature and penetrate the dense tumour tissue to reach the target tumour cells.

To achieve efficient delivery to the tumour core, it is essential to understand and address the specific challenges and requirements encountered at each stage of NP transport within the body.[257] Studies have demonstrated that negatively charged or neutral NPs exhibit faster diffusion rates *in vivo* compared to positively charged NPs. This difference is attributed to the tendency of positively charged NPs to interact with oppositely charged proteins and membrane structures within the extracellular matrix, leading to aggregation.[175,258,259] Conversely, positively charged NPs with sizes around 100 nm have been found to achieve superior tissue penetration in 3D tumour spheroid models and *in vivo* tumour environments compared to their negatively charged or neutral counterparts.[260,261] These findings highlight a fundamental dilemma in nanomedicine: optimising both effective accumulation at the tumour site and deep penetration into tumour tissue. Consequently, the development of surface charge-switchable drug delivery systems presents a promising strategy for enhancing the overall performance of nanoparticle-based therapies (Table 2).[173,262]

3.1 Core–shell nanoparticles

The design of core–shell structured NPs utilising stimuli-responsive core–shell separation mechanisms represent one of the most effective strategies for developing surface charge-switchable drug delivery systems. Upon accumulation at the tumour site, these specially engineered core–shell NPs can undergo separation of their core and shell components in response to external stimuli – such as light, ultrasound, or heat – or internal triggers, including variations in pH, enzyme expression, or the presence of specific biomolecules. This separation process enables the controlled modulation of surface charge, typically through the detachment of a negatively charged shell from the nanoparticle core.[25,172,174]

3.1.1 pH-Triggered charge reversal. Researchers commonly exploit electrostatic interactions to anchor negatively charged pH-responsive polymers onto the surface of positively charged NPs, thereby enabling pH-triggered deshelling behavior. For example, Chen *et al.*[173,290] developed structured supramolecular NPs by introducing an acid-responsive group, dimethyl maleic anhydride (DMMA), onto a polyamino acid polymer to form a pH-sensitive polymer shell (shell-DMMA). Through electrostatic interactions, this shell was assembled onto the surface of the SNPs. Upon accumulation within the acidic TME, the SNPs underwent a responsive "shell removal", leading to a substantial reduction in particle size (from approximately 145 nm to 40 nm) and a reversal of surface charge (from −7.4 mV to +8.2 mV). This structural transformation markedly enhanced the penetration of SNPs within tumour tissue (Fig. 17).

3.1.2 Enzyme-triggered charge reversal. In recent years, several tumour-specific enzymes present in the TME, such as matrix metalloproteinase-2 (MMP-2), hyaluronidase (HAase), and fibroblast activation protein-α (FAP-α), have been identified.[291,292] Building on this discovery, enzyme-responsive custom peptides have been widely utilised to develop enzyme-degradable nanoparticle carriers. For example, Kang *et al.*[293] reported a dual-responsive nanoparticle system (sNP@G/IR) capable of achieving deep tumour penetration and site-specific release of chemotherapeutic agents. The sNP@G/IR system is composed of a hyaluronic acid (HA) shell and a glutathione (GSH)-responsive polymeric core, encapsulating the anticancer drug gemcitabine (Gem) and the photothermal photosensitiser IR1048. The HA shell facilitates active tumour targeting by specifically binding to tumour markers such as CD44. Upon reaching the tumour microenvironment, the HA shell is degraded by hyaluronidase (HAase) present in the ECM, thereby exposing the positively charged inner core of the nanoparticle. This enzymatic degradation leads to a reduction in particle size and a reversal of surface charge, ultimately enhancing both tumour penetration and drug release efficiency of the sNP@G/IR system (Fig. 18).

3.1.3 Hypoxia-responsive charge reversal. Hypoxia is one of the most common and critical characteristics of solid malignant tumours.[294] While the oxygen tension in most normal tissues ranges from 40 to 60 mmHg, tumours with oxygen tensions below 10 mmHg are classified as hypoxic. This hypoxic state arises from an imbalance between oxygen supply and consumption within the tumour. Numerous studies have demonstrated that the hypoxic tumour microenvironment is closely associated with accelerated tumour progression and reduced overall patient survival.[295,296]

Therefore, the hypoxic microenvironment within tumours can be exploited to design charge-reversible NPs. For example, Chen *et al.*[277] developed a hypoxia-responsive nanoparticle system based on dendritic grafted polylysine (DGL), a positively charged nanocarrier (<10 nm, +50 mV), loaded with gemcitabine monophosphate (pGem). To improve circulation

Table 2 Different types of responsively charge-reversed NPs and its response mechanism

Type	Response mechanism	Structure change
pH-Responsive charge inversion	Unstable bonds under acidic conditions (pH 5.5–6.5) such as hydrazone (–C═N–NH–),[263] imine (–C═N–),[264] acetal/ketal (–CH(OR$_2$)(OR$_3$)),[265] others.[266] pI-based pH-responsive charge inversion: the protonation of the polymer[267,268] or peptides,[269,270] and pH-triggered deprotection of certain groups.[271]	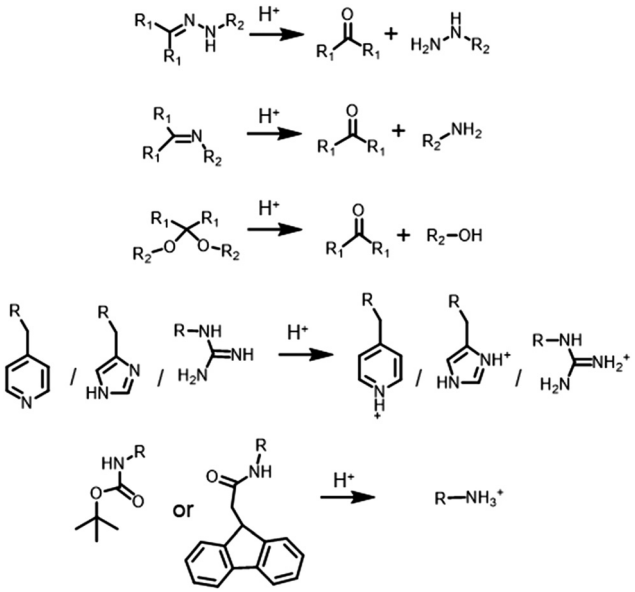
Enzyme-responsive charge inversion	Using peptides linker response to tumour-specific overexpressed enzymes such as metalloproteinases (MMP),[272–274] phospholipase A2 (PLA2),[275] γ-glutamyl transpeptidase[276]	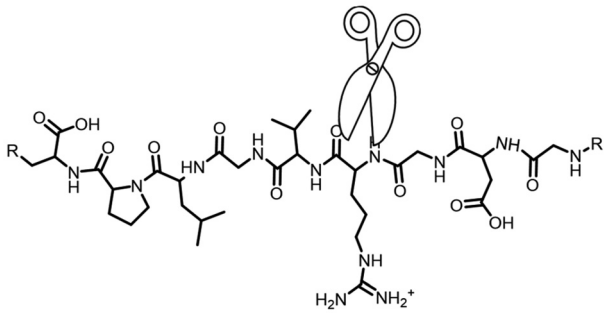
Hypoxia-responsive charge inversion	Using groups that are sensitive to hypoxic conditions: nitroimidazole,[277] azobenzene[278]	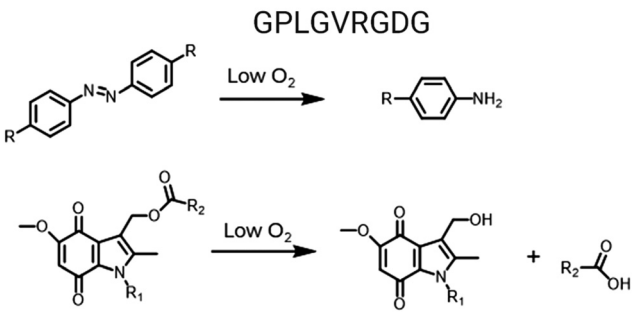
Ion-responsive charge inversion	Metal coordination: Ca^{2+} (osteosarcoma),[279] K^+ (ref. 280)	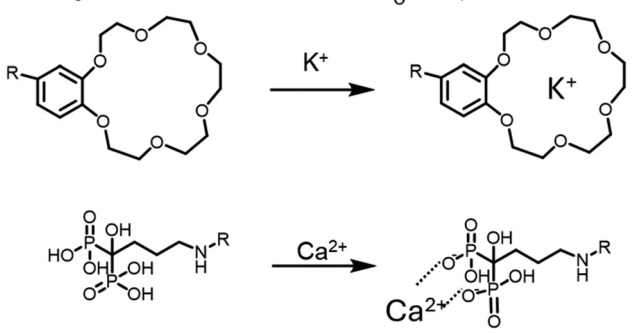

Table 2 *(Contd.)*

Type	Response mechanism	Structure change
Light-responsive charge inversion	Based on photosensitive molecules[281,282] or photo-unstable group such as *o*-nitrobenzyl,[283] others[284]	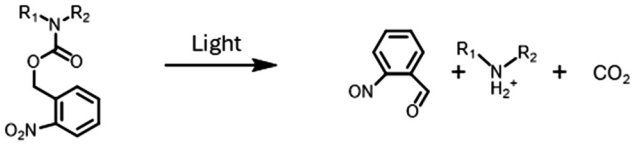
Redox/oxidative-responsive charge inversion	Responsive to reducing agents such as glutathione (GSH): disulfide (–S–S–).[285,286] ROS-responsive bond: thioketal bond (–C(SR_2)(SR_3)),[287] boronic acid,[288] others[289]	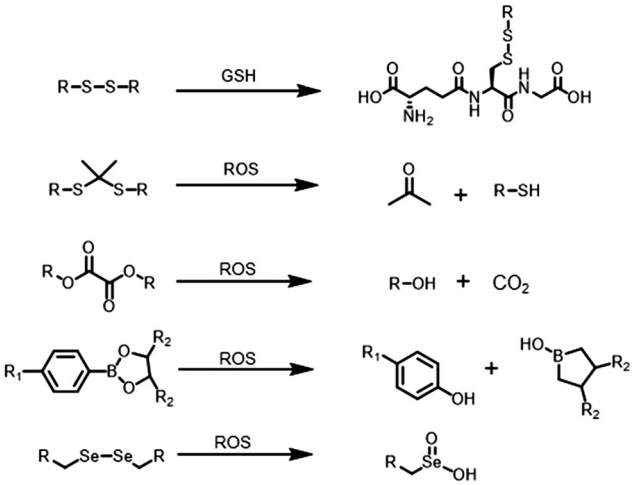

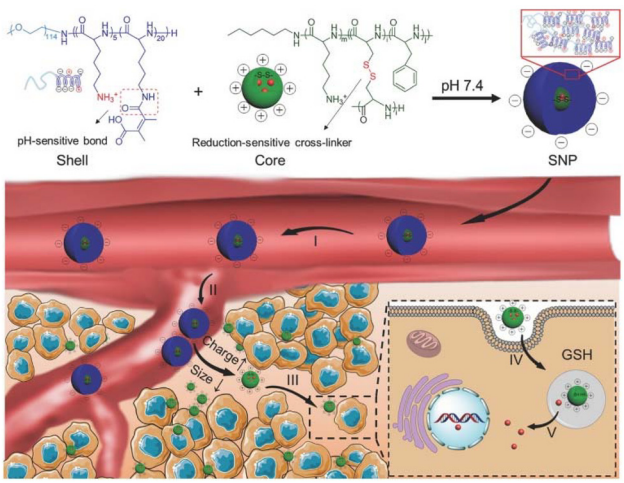

Fig. 17 Schematic illustration of the shell-stacked NPs, whose shell is formed *via* electrostatic interaction of dimethylmaleic anhydride-modified polypeptide (shell-DMMA), enabling sharp size reduction (from 145 nm to 40 nm) and charge reversal (from −7.4 mV to 8.2 mV) in the acidic tumour microenvironment. Adapted with permission ref. 290. Copyright 2017 John Wiley & Sons.

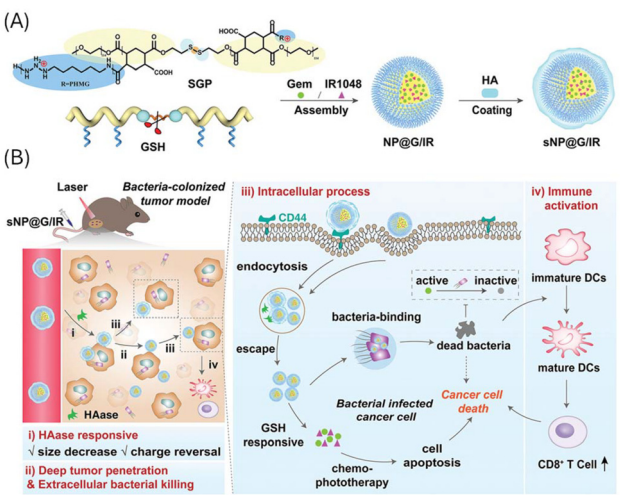

Fig. 18 (A) Schematic illustration of the dual-cascade responsive nanoparticle (sNP@G/IR) formed by loading Gem and IR1048 into an amphiphilic GSH-responsive polymer (SGP) and further coated with enzyme-responsive HA. (B) sNP@G/IR effectively targets and eliminates tumour-resident bacteria, delivers Gem and IR1048 for enhanced pancreatic cancer therapy, and boosts immune responses through a combination of bacterial killing, drug release, and laser-triggered hyperthermia. Adapted with permission ref. 293. Copyright 2022 John Wiley & Sons.

stability, DGL units were crosslinked into a mesh-like structure using a hypoxia-sensitive linker. The nanoparticles were further functionalised with the STAT3 inhibitor HJC0152 and coated with a negatively charged tenascin-C-targeting aptamer (GBI-10), which provided active tumour targeting while masking the positive surface charge to prolong systemic circulation. Upon reaching the hypoxic tumour microenvironment, the hypoxia-sensitive linker degraded, resulting in nanoparticle disassembly. The GBI-10 aptamer detached and bound to the tumour extracellular matrix, exposing the cationic DGL core. This exposure facilitated targeted release of HJC0152 and enhanced the tumour penetration of pGem, ultimately promoting immune activation and inducing cancer cell apoptosis (Fig. 19).

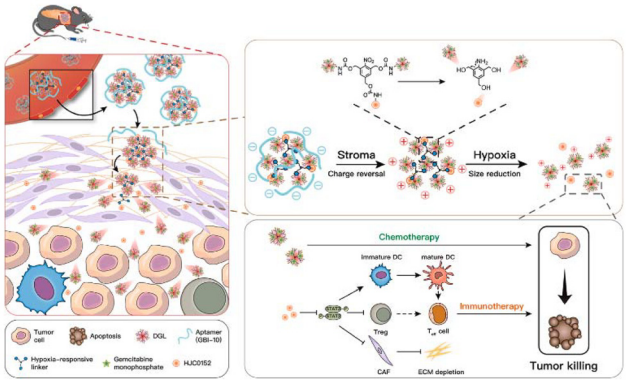

Fig. 19 Schematic illustration of dendri-graft poly-lysine (DGL) NPs cross-linked with a hypoxia-responsive ternary linker for targeted gemcitabine monophosphate (pGem) delivery. Upon tumour accumulation, the GBI-10 aptamer binds to the ECM, causing the release of the positively charged core. This process triggers size reduction and the release of HJC0152 in the hypoxic tumour microenvironment, enhancing the therapeutic effect. Adapted with permission ref. 277. Copyright 2022 Elsevier.

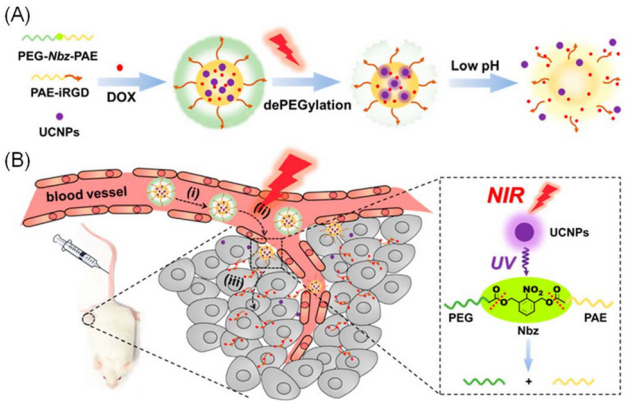

Fig. 20 (A) Schematic illustration of pH-sensitive NPs composed of PEG-Nbz-PAE-Nbz-PEG (HTMP) and iRGD-PAE-iRGD (iPHT) polymers, with UCNPs used for NIR-to-UV conversion, triggering cleavage of the Nbz linkers and dePEGylation, which (B) then activates iRGD for enhanced tumour penetration and drug release. Adapted with permission ref. 304. Copyright 2019 American Chemical Society.

3.1.4 Light-controlled charge reversal. It is known that although PEGylation effectively shields the surface charge of NPs and prolongs their systemic circulation, it also reduces cellular uptake and limits deep tumour penetration. To overcome this limitation, researchers have proposed the design of NPs capable of undergoing "PEG de-shielding" in response to specific stimuli. This is typically achieved by introducing cleavable chemical linkers between the PEG shell and the positively charged NP core, allowing for controlled removal of the PEG layer within the tumour microenvironment.[297] Several strategies for PEG shell removal in response to endogenous stimuli have been widely explored in recent years. However, accumulating evidence suggests that relying solely on endogenous factors such as pH shifts,[298,299] redox gradients,[300] and enzyme expression levels[301,302] can be hindered by individual patient variability, thereby limiting the clinical applicability of these stimuli-responsive NPs. In contrast, light-mediated modifications offer enhanced precision by enabling greater spatial and temporal control over therapeutic activation. Among various light sources, NIR light is particularly advantageous due to its superior tissue penetration and biocompatibility, making it an effective external trigger for PEG detachment and surface charge reversal.[303]

Zhou *et al.*[304] developed an amphiphilic polymer system composed of PEG as the hydrophilic segment and a pH-sensitive poly(β-amino ester) (PAE) as the hydrophobic segment, covalently linked *via* nitrobenzyl (Nbz) groups, forming PEG-Nbz-PAE-Nbz-PEG. In addition, a second amphiphilic polymer functionalised with iRGD peptides at both termini for tumour targeting, referred to as iRGD-PAE-iRGD (iPHT), was synthesised. These two polymers were co-assembled to encapsulate $NaYF_4$:Yb/Tm@$NaYF_4$, an upconversion nanoparticle capable of converting NIR light into UV-visible emissions. The resulting core–shell NPs enabled NIR light-triggered PEG shell removal upon accumulation in the tumour microenvironment. This process exposed the positively charged, iRGD-functionalised cores, leading to surface charge reversal and enhanced tumour penetration (Fig. 20).

3.2 Protonation-mediated charge reversal in tumour microenvironment

Polyetherimide (PEI) is widely utilised as a polymeric carrier for nucleic acid therapeutics. Beyond its strong electrostatic affinity for negatively charged small interfering RNA (siRNA) and its flexible chain structure, PEI exhibits a distinctive "proton sponge effect" under acidic conditions, facilitating the rapid escape of NPs from endosomes and the successful release of encapsulated nucleic acids into the cytoplasm.[305] The dense polyamine structure of PEI, characterised by a high density of closely spaced amino groups, endows it with excellent proton-buffering capacity across a broad pH range. For instance, as the pH decreases from 7.22 to 5.00, the degree of protonation of PEI amines increases from approximately 20% to 45%. Owing to this unique property, PEI has been extensively explored for the design of drug delivery systems capable of pH-responsive surface charge reversal.[306,307] Similar protonation reactions also occur in amino-substituted heterocycles.[308]

Li *et al.*[309] developed a PEI-based organic polymer NP system designed for pH-responsive behaviour (Fig. 21). Under physiological blood conditions (pH 7.4), the NPs maintained a negative surface charge, thereby achieving prolonged circulation times. Upon reaching the TME, where the pH is slightly acidic (approximately 6.8), increased protonation of PEI triggered a surface charge reversal from negative to positive. This charge switches enhanced NP uptake by tumour cells and promoted rapid drug release within endosomes. To further stabilise the PEI polymer and prevent premature degradation of the encapsulated nucleic acid drugs during systemic circulation,

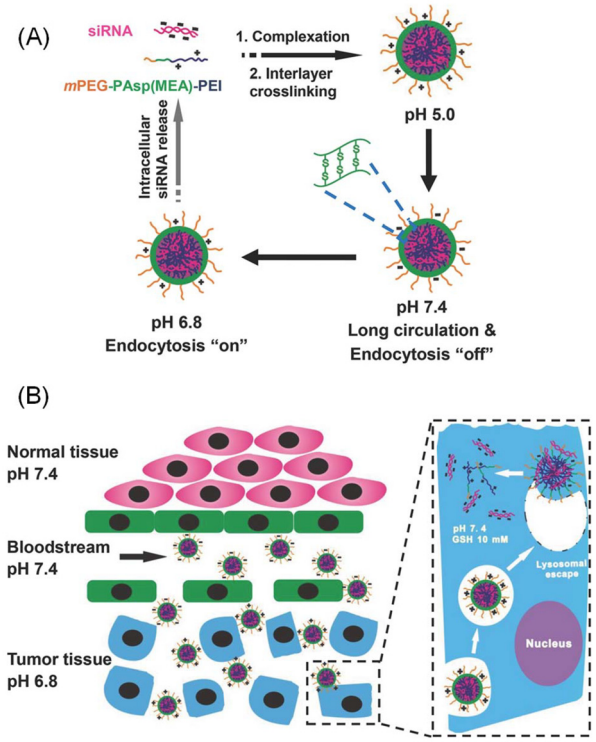

Fig. 21 (A) Schematic illustration of a surface charge-reversible polyplex composed of a pH-buffering PEI core complexed with siRNA, a PEG corona, and a reduction-sensitive disulfide-crosslinked interlayer. (B) The polyplex is negatively charged in blood circulation (pH = 7.4), becomes positively charged in tumour tissue (pH = 6.8) for cell uptake, and further turns positively charged in lysosomes (pH = 5) to facilitate lysosomal escape. Adapted with permission ref. 309. Copyright 2014 John Wiley & Sons.

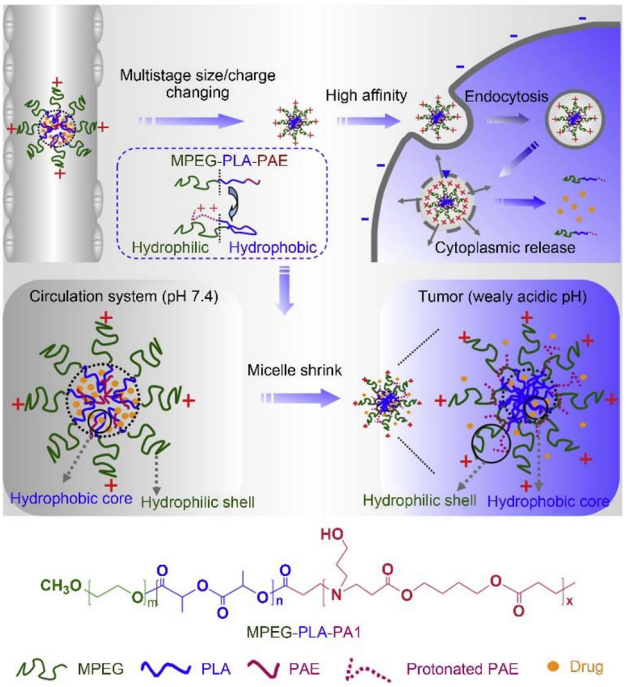

Fig. 22 Schematic illustration of a multistage drug delivery system using amphiphilic and pH-sensitive MPEG-PLA-PAE copolymers for curcumin (CUR) delivery, which shrinks from 171.0 nm to 22.6 nm and increasing surface charge to 24.8 mV in response to the acidic tumour microenvironment, leading to enhanced CUR cellular uptake and tumour accumulation. Adapted with permission ref. 311. Copyright 2014 Elsevier.

the PEI/siRNA complex was additionally encapsulated within a redox-sensitive polymer, forming a more robust nanostructure. Experimental results demonstrated that the PEI/siRNA complex remained stable in the bloodstream, while the pH-triggered charge reversal at the tumour site effectively silenced tumour-specific genes. In contrast, in normal tissues lacking an acidic microenvironment, the complex retained its negative charge, resulting in minimal siRNA uptake by healthy cells and significantly reducing off-target gene transfection. These findings highlight the substantial potential of charge-reversal strategies for the design of gene delivery systems.

Poly(β-amino ester) (PAE) is a pH-responsive, biodegradable polymer that remains insoluble in aqueous environments at higher pH values (*e.g.*, pH 7.4) but dissolves under lower pH conditions due to the protonation of its tertiary amine groups. Wang *et al.*[310] reported the development of several pH-responsive NPs, all incorporating protonatable tertiary amine functionalities that enable responsiveness to different pH environments (Fig. 22). These NPs were fabricated using PEG-*b*-poly(2-(*N*-methylacrylamido)ethyl methacrylate)-modified polyamide PAMAM dendrimers (PEG-*b*-PAEMA-PAMAM), with an average size of approximately 80 nm and an extended blood circulation time at physiological pH (7.8). Upon reaching the acidic TME, the protonation of the tertiary amine groups in PAMAM triggered NP disassembly into highly cationic dendritic molecular structures, significantly enhancing their penetration into the tumour core. Additionally, size- and charge-adaptable stimuli-responsive drug delivery systems have been developed to further improve delivery efficacy. Nanomicelles formed from a blend of MPEG-PLA (methoxy poly(ethylene glycol)-poly(lactic acid)) and PAE demonstrated superior tissue penetration after extravasation from tumour vasculature compared to micelles composed solely of MPEG-PLA copolymers. This enhanced penetration was attributed to the protonation of PAE chains in the acidic TME, which induced simultaneous changes in both the size and surface charge of the micelles, ultimately increasing the uptake of the loaded drug, curcumin, by tumour cells.[311]

4. Conclusion

Nanoparticle-based drug delivery systems have made significant progress in advancing precision medicine, especially in the treatment of cancer. Drug delivery systems that respond to the distinct features of the TME, such as variations in pH, redox potential, or enzymatic activity, have attracted considerable attention for their potential to enhance therapeutic efficacy while minimising systemic toxicity. Despite these advances, achieving deep and uniform penetration of NPs

within tumour tissues remains a critical challenge, significantly limiting the overall effectiveness of nanoparticle-based therapies. To address this limitation, a variety of strategies have been developed, including size-adaptable designs, surface modifications, charge-reversal mechanisms, and shape-transformable nanoparticles. One of the most significant advances in this field is the development of charge-reversal nanoparticles. These nanoparticles are designed to undergo a charge reversal in response to specific environmental stimuli, such as the acidic pH characteristic of the TME, or other factors such as redox conditions. The ability to reverse charge provides several key advantages: enhanced tumour penetration, prolonged circulation time, and reduced off-target toxicity.

Despite these encouraging developments, significant challenges must be addressed to fully realise the potential of charge-reversal nanoparticles and successfully transition them from laboratory concepts to clinical trials. Many reported systems rely on non-biodegradable or non-FDA-approved materials that compromise biocompatibility and regulatory approval, ultimately limiting their clinical applicability. In addition, many systems exhibit suboptimal charge conversion amplitudes, which may be insufficient to enable effective membrane interaction, cellular uptake, or endosomal escape.[312] Furthermore, off-target accumulation in organs such as the liver, spleen, and lungs not only reduces therapeutic efficacy but also raises toxicity concerns. Additionally, protein corona formation in biological fluids can obscure nanoparticle surfaces, impairing targeting precision and drug release.[313]

To overcome these challenges, future development of charge-reversal nanoparticles should prioritise the use of biocompatible, biodegradable, and clinically approved materials, such as naturally derived polyanions, *e.g.*, hyaluronic acid or alginate, or FDA-approved polymers such as poly(lactic-*co*-glycolic acid) (PLGA).[95] Enhancing the magnitude and responsiveness of charge conversion can be achieved through rational design of cleavable surface chemistries that respond more efficiently to well-defined biological triggers such as acidic pH, elevated glutathione, or tumour-specific enzymes. Incorporating time-triggered or multi-stimuli-responsive elements may provide more consistent activation in heterogeneous tumour microenvironments. To address off-target accumulation, surface engineering techniques, such as PEGylation, zwitterionic coatings, or biomimetic cloaking, can improve circulation time and reduce recognition by the phagocyte system. In parallel, the design of stealth coatings that resist protein adsorption can minimise protein corona formation and preserve nanoparticle functionality *in vivo*. Ultimately, integrating these strategies will support the development of charge-reversal nanoparticles with enhanced therapeutic efficacy and improved clinical translation potential.

Author contributions

Conceptualisation, J. Z. and V. A. B.; writing – original draft, J. Z., G. W. and V. A. B.; writing – review & editing, J. Z., G. W. and V. A. B.; project administration and supervision, V. A. B.

Conflicts of interest

There are no conflicts to declare.

Data availability

Data availability is not applicable to this article as no new data were created or analysed in this study.

References

1 M. R. Zalutsky, *J. Nucl. Med.*, 2005, **46**, 151S.
2 W. A. Weber, *J. Nucl. Med.*, 2009, **50**, 1S.
3 A. K. Ilkay, G. W. Chodak, N. J. Vogelzang and G. S. Gerber, *Urology*, 1993, **42**, 599–602.
4 Q. Luo, L. Zhang, C. Luo and M. Jiang, *Cancer Lett.*, 2019, **454**, 191–203.
5 D. Long, T. Liu, L. Tan, H. Shi, P. Liang, S. Tang, Q. Wu, J. Yu, J. Dou and X. Meng, *ACS Nano*, 2016, **10**, 9516–9528.
6 W. E. Gutteridge, *Br. Med. Bull.*, 1985, **41**, 162–168.
7 E. Pérez-Herrero and A. Fernández-Medarde, *Eur. J. Pharm. Biopharm.*, 2015, **93**, 52–79.
8 X.-J. Liang, C. Chen, Y. Zhao and P. C. Wang, in *Multi-Drug Resistance in Cancer*, ed. J. Zhou, Humana Press, Totowa, NJ, 2010, pp. 467–488, DOI: 10.1007/978-1-60761-416-6_21.
9 F.-S. Liu, *Taiwan. J. Obstet. Gynecol.*, 2009, **48**, 239–244.
10 F. Shakeel, *Molecules*, 2023, **28**, 4138.
11 S. M. Roy, V. Garg, S. P. Sivaraman, S. Barman, C. Ghosh, P. Bag, P. Mohanasundaram, P. S. Maji, A. Basu, A. Dirisala, S. K. Ghosh and A. R. Maity, *J. Drug Delivery Sci. Technol.*, 2023, **83**, 104408.
12 R. Bazak, M. Houri, S. El Achy, W. Hussein and T. Refaat, *Mol. Clin. Oncol.*, 2014, **2**, 904–908.
13 M. F. Attia, N. Anton, J. Wallyn, Z. Omran and T. F. Vandamme, *J. Pharm. Pharmacol.*, 2019, **71**, 1185–1198.
14 F. Danhier, O. Feron and V. Préat, *J. Controlled Release*, 2010, **148**, 135–146.
15 S. M. Ryan and D. J. Brayden, *Curr. Opin. Pharmacol.*, 2014, **18**, 120–128.
16 B. Chen, W. Dai, B. He, H. Zhang, X. Wang, Y. Wang and Q. Zhang, *Theranostics*, 2017, **7**, 538–558.
17 F. u. Din, A. Waqar, U. Izhar, Q. O. Salman, M. Omer, S. Shumaila and A. Zeb, *Int. J. Nanomed.*, 2017, **12**, 7291–7309.
18 B. He, S. Xin, Y. Bing, W. Song, S. Youqing and H. Cong, *Drug Delivery*, 2020, **27**, 1474–1490.
19 F. Chen, X. Zhuang, L. Lin, P. Yu, Y. Wang, Y. Shi, G. Hu and Y. Sun, *BMC Med.*, 2015, **13**, 45.

20 H. Maeda, J. Wu, T. Sawa, Y. Matsumura and K. Hori, *J. Controlled Release*, 2000, **65**, 271–284.
21 D. Ling, M. J. Hackett and T. Hyeon, *Nano Today*, 2014, **9**, 457–477.
22 L. Sun, Q. Wu, F. Peng, L. Liu and C. Gong, *Colloids Surf., B*, 2015, **135**, 56–72.
23 W. Yu, R. Liu, Y. Zhou and H. Gao, *ACS Cent. Sci.*, 2020, **6**, 100–116.
24 Y. Xu, T. Fourniols, Y. Labrak, V. Préat, A. Beloqui and A. des Rieux, *ACS Nano*, 2022, **16**, 7168–7196.
25 Y. Hu, X. Gong, J. Zhang, F. Chen, C. Fu, P. Li, L. Zou and G. Zhao, *Polymer*, 2016, **8**, 99.
26 B. Romberg, W. E. Hennink and G. Storm, *Pharm. Res.*, 2008, **25**, 55–71.
27 Z.-G. Yue, W. Wei, P.-P. Lv, H. Yue, L.-Y. Wang, Z.-G. Su and G.-H. Ma, *Biomacromolecules*, 2011, **12**, 2440–2446.
28 J.-b. Du, Y. Cheng, Z.-h. Teng, M.-l. Huan, M. Liu, H. Cui, B.-l. Zhang and S.-y. Zhou, *Mol. Pharm.*, 2016, **13**, 1711–1722.
29 Y. Liping, J. He, Z. Tao, Y. Zhou, J. Yang, Y. Zhang, J. Gao and Q. Liting, *Drug Delivery*, 2022, **29**, 229–237.
30 S. Sandhiya, S. A. Dkhar and A. Surendiran, *Fundam. Clin. Pharmacol.*, 2009, **23**, 263–269.
31 M. Hu, X. Li, Z. You, R. Cai and C. Chen, *Adv. Mater.*, 2024, **36**, 2303266.
32 R. Tenchov, R. Bird, A. E. Curtze and Q. Zhou, *ACS Nano*, 2021, **15**, 16982–17015.
33 S. Sheoran, S. Arora, R. Samsonraj, P. Govindaiah and S. Vuree, *Heliyon*, 2022, **8**, e09403.
34 S. Samimi, N. Maghsoudnia, R. B. Eftekhari and F. Dorkoosh, in *Characterization and Biology of Nanomaterials for Drug Delivery*, ed. S. S. Mohapatra, S. Ranjan, N. Dasgupta, R. K. Mishra and S. Thomas, Elsevier, 2019, pp. 47–76, DOI: 10.1016/B978-0-12-814031-4.00003-9.
35 A. D. Miller, *J. Drug Delivery*, 2013, **2013**, 165981.
36 M. A. Obeid, R. J. Tate, A. B. Mullen and V. A. Ferro, in *Lipid Nanocarriers for Drug Targeting*, ed. A. M. Grumezescu, William Andrew Publishing, 2018, pp. 313–359, DOI: 10.1016/B978-0-12-813687-4.00008-6.
37 W.-L. Tang, W.-H. Tang and S.-D. Li, *Drug Discovery Today*, 2018, **23**, 1159–1166.
38 Z. R. Cohen, S. Ramishetti, N. Peshes-Yaloz, M. Goldsmith, A. Wohl, Z. Zibly and D. Peer, *ACS Nano*, 2015, **9**, 1581–1591.
39 L. Wayteck, H. Dewitte, L. De Backer, K. Breckpot, J. Demeester, S. C. De Smedt and K. Raemdonck, *Biomaterials*, 2016, **77**, 243–254.
40 L. C. Gomes-da-Silva, N. A. Fonseca, V. Moura, M. C. Pedroso de Lima, S. Simões and J. N. Moreira, *Acc. Chem. Res.*, 2012, **45**, 1163–1171.
41 C. Horejs, *Nat. Rev. Mater.*, 2021, **6**, 1075–1076.
42 X. Hou, T. Zaks, R. Langer and Y. Dong, *Nat. Rev. Mater.*, 2021, **6**, 1078–1094.
43 S. Santra, S. Das, S. Dey, A. Sengupta, B. Giri and M. R. Molla, *Biomacromolecules*, 2024, **25**, 1724–1737.
44 S. Kolay, M. Das, A. Mondal, A. Sengupta, S. Bag, P. De and M. R. Molla, *Biomacromolecules*, 2024, **25**, 5068–5080.
45 M. A. Beach, U. Nayanathara, Y. Gao, C. Zhang, Y. Xiong, Y. Wang and G. K. Such, *Chem. Rev.*, 2024, **124**, 5505–5616.
46 R. H. Prabhu and V. B. Patravale, *Int. J. Nanomed.*, 2015, **10**, 1001–1018.
47 S. A. Dilliard and D. J. Siegwart, *Nat. Rev. Mater.*, 2023, **8**, 282–300.
48 Y. L. Colson and M. W. Grinstaff, *Adv. Mater.*, 2012, **24**, 3878–3886.
49 T. Senthilkumar, L. Zhou, Q. Gu, L. Liu, F. Lv and S. Wang, *Angew. Chem., Int. Ed.*, 2018, **57**, 13114–13119.
50 R. Cheng, F. Meng, C. Deng, H.-A. Klok and Z. Zhong, *Biomaterials*, 2013, **34**, 3647–3657.
51 K. S. Soppimath, D. C. W. Tan and Y. Y. Yang, *Adv. Mater.*, 2005, **17**, 318–323.
52 A. P. Griset, J. Walpole, R. Liu, A. Gaffey, Y. L. Colson and M. W. Grinstaff, *J. Am. Chem. Soc.*, 2009, **131**, 2469–2471.
53 Y.-Y. Yuan, C.-Q. Mao, X.-J. Du, J.-Z. Du, F. Wang and J. Wang, *Adv. Mater.*, 2012, **24**, 5476–5480.
54 J. Zhang, H. Sun and P. X. Ma, *ACS Nano*, 2010, **4**, 1049–1059.
55 M. Aquib, S. Schaefer, H. Gmedhin, N. Corrigan, V. A. Bobrin and C. Boyer, *Eur. Polym. J.*, 2024, **205**, 112698.
56 V. A. Bobrin, S.-P. R. Chen, C. F. Grandes Reyes, T. Smith, D. F. J. Purcell, J. Armstrong, J. L. McAuley and M. J. Monteiro, *Biomacromolecules*, 2022, **23**, 3960–3967.
57 Z. A. I. Mazrad, B. Schelle, J. A. Nicolazzo, M. N. Leiske and K. Kempe, *Biomacromolecules*, 2021, **22**, 4618–4632.
58 P. Wei, G. Gangapurwala, D. Pretzel, M. N. Leiske, L. Wang, S. Hoeppener, S. Schubert, J. C. Brendel and U. S. Schubert, *Biomacromolecules*, 2019, **20**, 130–140.
59 S. Bhattacharya, B. G. Prajapati and S. Singh, *Crit. Rev. Oncol. Hematol.*, 2023, **185**, 103961.
60 P. Sakore, S. Bhattacharya, S. Belemkar, B. G. Prajapati and G. M. Elossaily, *Results Chem.*, 2024, **7**, 101264.
61 Z. Tang, Q. He, J. Zhou, S. Yan, L. Jiang, Y. Wang, C. Yao, H. Wei, K. Yang and J. Wang, *Chin. Chem. Lett.*, 2024, **35**, 109742.
62 J. Y. Oh, M.-S. Seu, A. K. Barui, H. W. Ok, D. Kim, E. Choi, J. Seong, M. S. Lah and J.-H. Ryu, *Nanoscale*, 2024, **16**, 14748–14756.
63 Q. Wang and D. Astruc, *Chem. Rev.*, 2020, **120**, 1438–1511.
64 D. C. Luther, R. Huang, T. Jeon, X. Zhang, Y.-W. Lee, H. Nagaraj and V. M. Rotello, *Adv. Drug Delivery Rev.*, 2020, **156**, 188–213.
65 H. Mattoussi and V. M. Rotello, *Adv. Drug Delivery Rev.*, 2013, **65**, 605–606.
66 M. Liong, J. Lu, M. Kovochich, T. Xia, S. G. Ruehm, A. E. Nel, F. Tamanoi and J. I. Zink, *ACS Nano*, 2008, **2**, 889–896.
67 S. Wuttke, M. Lismont, A. Escudero, B. Rungtaweevoranit and W. J. Parak, *Biomaterials*, 2017, **123**, 172–183.

68 R. Mohammapdour and H. Ghandehari, *Adv. Drug Delivery Rev.*, 2022, **180**, 114022.
69 M. Ding, W. Liu and R. Gref, *Adv. Drug Delivery Rev.*, 2022, **190**, 114496.
70 M.-X. Wu and Y.-W. Yang, *Adv. Mater.*, 2017, **29**, 1606134.
71 S. He, L. Wu, X. Li, H. Sun, T. Xiong, J. Liu, C. Huang, H. Xu, H. Sun, W. Chen, R. Gref and J. Zhang, *Acta Pharm. Sin. B*, 2021, **11**, 2362–2395.
72 Q. Li, X. Yang, X. Xia, X.-X. Xia and D. Yan, *Biomacromolecules*, 2024, **25**, 6474–6484.
73 M. Kumar, A. Jha and B. Mishra, *Chem Bio Eng.*, 2024, **1**, 179–198.
74 M. Nair, A. Chandra, A. Krishnan, A. Chandra, R. Basha, H. Orimoloye, S. Raut, V. Gayathri, V. V. Mudgapalli and J. K. Vishwanatha, in *Nanostructured Materials for Biomedical Applications*, ed. R. Vijayamma, N. Kalarikkal and S. Thomas, Elsevier, 2024, pp. 339–404, DOI: 10.1016/B978-0-323-90838-2.00011-4.
75 Y. Zhang, T. Sun and C. Jiang, *Acta Pharm. Sin. B*, 2018, **8**, 34–50.
76 K. A. Dawson and Y. Yan, *Nat. Mater.*, 2016, **15**, 935–936.
77 Y. Xie, C. Ma, X. Yang, J. Wang, G. Long and J. Zhou, *Adv. Drug Delivery Rev.*, 2021, **176**, 113868.
78 B. Zhao, L. Li, X. Lv, J. Du, Z. Gu, Z. Li, L. Cheng, C. Li and Y. Hong, *J. Controlled Release*, 2022, **349**, 662–678.
79 C. Wiraja, Y. Zhu, D. C. S. Lio, D. C. Yeo, M. Xie, W. Fang, Q. Li, M. Zheng, M. Van Steensel, L. Wang, C. Fan and C. Xu, *Nat. Commun.*, 2019, **10**, 1147.
80 Z. Jin, G. Hu and K. Zhao, *Carbohydr. Polym.*, 2022, **283**, 119174.
81 V. R. Kohout, C. L. Wardzala and J. R. Kramer, *Adv. Drug Delivery Rev.*, 2022, **191**, 114540.
82 Z. S. Clauss and J. R. Kramer, *Adv. Drug Delivery Rev.*, 2021, **169**, 152–167.
83 J. Kaltbeitzel and P. R. Wich, *Angew. Chem., Int. Ed.*, 2023, **62**, e202216097.
84 A. J. Dehchani, A. Jafari and F. Shahi, *Polym. Adv. Technol.*, 2024, **35**, e6595.
85 Z. Dai, X. Li, Q. Chen, Y. Zhu, Z. Shi, X. Deng, C. Wang and H. Chen, *Adv. Funct. Mater.*, 2024, **34**, 2313723.
86 N. Parsana, O. E. Seoud, A. Al-Ghamdi, N. Kasoju and N. Malek, *ChemistrySelect*, 2024, **9**, e202304157.
87 N. H. Thang, T. B. Chien and D. X. Cuong, *Gels*, 2023, **9**, 523.
88 J. Li and D. J. Mooney, *Nat. Rev. Mater.*, 2016, **1**, 16071.
89 S. Bernhard and M. W. Tibbitt, *Adv. Drug Delivery Rev.*, 2021, **171**, 240–256.
90 F. Rizzo and N. S. Kehr, *Adv. Healthcare Mater.*, 2021, **10**, 2001341.
91 Y. Qiu and K. Park, *Adv. Drug Delivery Rev.*, 2012, **64**, 49–60.
92 M. Hamidi, A. Azadi and P. Rafiei, *Adv. Drug Delivery Rev.*, 2008, **60**, 1638–1649.
93 H. Yu, R. Gao, Y. Liu, L. Fu, J. Zhou and L. Li, *Adv. Sci.*, 2024, **11**, 2306152.
94 Z. Wei, E. Volkova, M. R. Blatchley and S. Gerecht, *Adv. Drug Delivery Rev.*, 2019, **149–150**, 95–106.
95 D. Bobo, K. J. Robinson, J. Islam, K. J. Thurecht and S. R. Corrie, *Pharm. Res.*, 2016, **33**, 2373–2387.
96 N. Desai, D. Rana, M. Patel, N. Bajwa, R. Prasad and L. K. Vora, *Small*, 2025, **21**, 2502315.
97 R. Xu, A. Rai, M. Chen, W. Suwakulsiri, D. W. Greening and R. J. Simpson, *Nat. Rev. Clin. Oncol.*, 2018, **15**, 617–638.
98 X. Zhang, H. Zhang, J. Gu, J. Zhang, H. Shi, H. Qian, D. Wang, W. Xu, J. Pan and H. A. Santos, *Adv. Mater.*, 2021, **33**, 2005709.
99 A. Sharma and U. S. Sharma, *Int. J. Pharm.*, 1997, **154**, 123–140.
100 S. Deshpande, S. Wunnava, D. Hueting and C. Dekker, *Small*, 2019, **15**, 1902898.
101 D. E. Large, R. G. Abdelmessih, E. A. Fink and D. T. Auguste, *Adv. Drug Delivery Rev.*, 2021, **176**, 113851.
102 Y. Li, T. Ji, M. Torre, R. Shao, Y. Zheng, D. Wang, X. Li, A. Liu, W. Zhang, X. Deng, R. Yan and D. S. Kohane, *Nat. Commun.*, 2023, **14**, 6659.
103 S. Pande, *Artif. Cells, Nanomed., Biotechnol.*, 2023, **51**, 428–440.
104 H. Yoshioka, *Biomaterials*, 1991, **12**, 861–864.
105 M. Dymek and E. Sikora, *Adv. Colloid Interface Sci.*, 2022, **309**, 102757.
106 D. Patel, J. Solanki, M. M. Kher and A. Azagury, *Small*, 2024, **20**, 2401990.
107 D. Pasarin, A.-I. Ghizdareanu, C. E. Enascuta, C. B. Matei, C. Bilbie, L. Paraschiv-Palada and P.-A. Veres, *Polymers*, 2023, **15**, 782.
108 X. Han, Y. Cheng, D. Wan, A. Alu, Z. Zhang, Z. Bi, M. Wang, Y. Tang, W. Hong, S. Chen, L. Chen and Y. Wei, *Cancer Commun.*, 2025, **45**, 794–812.
109 L. Coderch, J. Fonollosa, M. De Pera, J. Estelrich, A. De La Maza and J. L. Parra, *J. Controlled Release*, 2000, **68**, 85–95.
110 E.-J. Go, H. Yang, W. Park, S. J. Lee, J.-H. Han, S. J. Kong, W. S. Lee, D. K. Han, H. J. Chon and C. Kim, *Small*, 2023, **19**, 2300544.
111 Z. Gao, J. Zhang, Y. Hou, J. Lu, J. Liang, Y. Gao, B. Li, S. Gao, Y. Zhao, M. Gao and J. Chen, *Biomaterials*, 2024, **305**, 122442.
112 S. S. Nunes, R. S. Fernandes, C. H. Cavalcante, I. da Costa César, E. A. Leite, S. C. A. Lopes, A. Ferretti, D. Rubello, D. M. Townsend, M. C. de Oliveira, V. N. Cardoso and A. L. B. de Barros, *Drug Delivery Transl. Res.*, 2019, **9**, 123–130.
113 Q. Du, Y. Liu, M. Fan, S. Wei, M. Ismail and M. Zheng, *J. Controlled Release*, 2024, **372**, 85–94.
114 X. Wang, N. Meng, S. Wang, Y. Zhang, L. Lu, R. Wang, H. Ruan, K. Jiang, H. Wang, D. Ran, C. Zhan, K. Yu, D. J. Burgess and W. Lu, *J. Controlled Release*, 2019, **316**, 381–392.
115 L. Zou, W. Ding, Y. Zhang, S. Cheng, F. Li, R. Ruan, P. Wei and B. Qiu, *Biomaterials*, 2018, **182**, 1–12.

116 M. Abri Aghdam, R. Bagheri, J. Mosafer, B. Baradaran, M. Hashemzaei, A. Baghbanzadeh, M. de la Guardia and A. Mokhtarzadeh, *J. Controlled Release*, 2019, **315**, 1–22.
117 T. Ta and T. M. Porter, *J. Controlled Release*, 2013, **169**, 112–125.
118 S. L. Huang, D. D. McPherson and R. C. Macdonald, *Ultrasound Med. Biol.*, 2008, **34**, 1272–1280.
119 S. Wang, G. Yu, W. Yang, Z. Wang, O. Jacobson, R. Tian, H. Deng, L. Lin and X. Chen, *Adv. Sci.*, 2021, **8**, 2002927.
120 S. E. Alavi, S. Alharthi, S. Z. Alavi, A. Raza and H. Ebrahimi Shahmabadi, *Drug Discovery Today*, 2024, **29**, 103849.
121 B. L. Banik, P. Fattahi and J. L. Brown, *WIREs Nanomed. Nanobiotechnol.*, 2016, **8**, 271–299.
122 J. M. Morachis, E. A. Mahmoud and A. Almutairi, *Pharmacol. Rev.*, 2012, **64**, 505–519.
123 Z. Zhang, P.-C. Tsai, T. Ramezanli and B. B. Michniak-Kohn, *WIREs Nanomed. Nanobiotechnol.*, 2013, **5**, 205–218.
124 M. Ye, Y. Han, J. Tang, Y. Piao, X. Liu, Z. Zhou, J. Gao, J. Rao and Y. Shen, *Adv. Mater.*, 2017, **29**, 1702342.
125 C. Y. Ang, S. Y. Tan, C. Teh, J. M. Lee, M. F. E. Wong, Q. Qu, L. Q. Poh, M. Li, Y. Zhang, V. Korzh and Y. Zhao, *Small*, 2017, **13**, 1602379.
126 P. Wang, Q. Gong, J. Hu, X. Li and X. Zhang, *J. Med. Chem.*, 2021, **64**, 298–325.
127 D. M. Bollag, P. A. McQueney, J. Zhu, O. Hensens, L. Koupal, J. Liesch, M. Goetz, E. Lazarides and C. M. Woods, *Cancer Res.*, 1995, **55**, 2325.
128 Y.-J. Zhu and F. Chen, *Chem. – Asian J.*, 2015, **10**, 284–305.
129 M. Zhang, N. Ying, J. Chen, L. Wu, H. Liu, S. Luo and D. Zeng, *Cell Proliferation*, 2024, **57**, e13603.
130 C. Yang, Z. Xue, Y. Liu, J. Xiao, J. Chen, L. Zhang, J. Guo and W. Lin, *Mater. Sci. Eng., C*, 2018, **84**, 254–262.
131 W. Ni, L. Zhang, H. Zhang, C. Zhang, K. Jiang and X. Cao, *Inorg. Chem.*, 2022, **61**, 3281–3287.
132 M. Moharramnejad, A. Ehsani, M. Shahi, S. Gharanli, H. Saremi, R. E. Malekshah, Z. S. Basmenj, S. Salmani and M. Mohammadi, *J. Drug Delivery Sci. Technol.*, 2023, **81**, 104285.
133 P. Wang, M. Xiao, H. Pei, H. Xing, S.-H. Luo, C.-K. Tsung and L. Li, *Chem. Eng. J.*, 2021, **415**, 129036.
134 Y. Zou, B. Huang, L. Cao, Y. Deng and J. Su, *Adv. Mater.*, 2021, **33**, 2005215.
135 J. Parra-Nieto, M. A. G. del Cid, I. A. de Cárcer and A. Baeza, *Biotechnol. J.*, 2021, **16**, 2000150.
136 X. Wang, X. Zhong, J. Li, Z. Liu and L. Cheng, *Chem. Soc. Rev.*, 2021, **50**, 8669–8742.
137 G. Choi, N. S. Rejinold, H. Piao and J.-H. Choy, *Chem. Sci.*, 2021, **12**, 5044–5063.
138 K. Chen, L. Cai, S. Yang, S. Peng, J. Huang, J. Xu, Z. Lu, X. Xu, B. Fu, L. Zhang and X. Zhou, *ACS Appl. Bio Mater.*, 2021, **4**, 4841–4848.
139 M. Cheng and H. Dou, *Polym. Int.*, 2022, **71**, 371–378.
140 Y. Hong, F. Zhou, Y. Hua, X. Zhang, C. Ni, D. Pan, Y. Zhang, D. Jiang, L. Yang, Q. Lin, Y. Zou, D. Yu, D. E. Arnot, X. Zou, L. Zhu, S. Zhang and H. Ouyang, *Nat. Commun.*, 2019, **10**, 2060.
141 S. Jafari, E. Ahmadian, J. K. Fard and A. Yari Khosroushahi, *J. Drug Delivery Sci. Technol.*, 2017, **37**, 61–66.
142 D. E. Sansonno, P. DeTomaso, M. A. Papanice and O. G. Manghisi, *J. Immunol. Methods*, 1986, **90**, 131–136.
143 Y. Xu, J. Xu, X. Hu, X. Xia, Q. Dong, Z. Liu, Z. Chen and W. Tan, *Nano Res.*, 2019, **12**, 1880–1887.
144 A. Chyzy, M. Tomczykowa and M. E. Plonska-Brzezinska, *Materials*, 2020, **13**, 188.
145 M. Akram and R. Hussain, in *Nanocellulose and Nanohydrogel Matrices*, 2017, pp. 297–330, DOI: 10.1002/9783527803835.ch11.
146 F. Damiri, A. Fatimi, A. C. P. Santos, R. S. Varma and M. Berrada, *J. Mater. Chem. B*, 2023, **11**, 10538–10565.
147 A. P. Mathew, S. Uthaman, K.-H. Cho, C.-S. Cho and I.-K. Park, *Int. J. Biol. Macromol.*, 2018, **110**, 17–29.
148 A. Riedinger, M. Pernia Leal, S. R. Deka, C. George, I. R. Franchini, A. Falqui, R. Cingolani and T. Pellegrino, *Nano Lett.*, 2011, **11**, 3136–3141.
149 Y. Jiang, J. Chen, C. Deng, E. J. Suuronen and Z. Zhong, *Biomaterials*, 2014, **35**, 4969–4985.
150 A. Basu, K. R. Kunduru, S. Doppalapudi, A. J. Domb and W. Khan, *Adv. Drug Delivery Rev.*, 2016, **107**, 192–205.
151 Y. Sheng, J. Gao, Z.-Z. Yin, J. Kang and Y. Kong, *Carbohydr. Polym.*, 2021, **269**, 118325.
152 N. M. Anderson and M. C. Simon, *Curr. Biol.*, 2020, **30**, R921–R925.
153 T. L. Whiteside, *Oncogene*, 2008, **27**, 5904–5912.
154 J. A. Joyce, *Cancer Cell*, 2005, **7**, 513–520.
155 P. A. Kenny, G. Y. Lee and M. J. Bissell, *Front. Biosci.*, 2007, **12**, 3468–3474.
156 K. Greish, in *Cancer Nanotechnology: Methods and Protocols*, ed. S. R. Grobmyer and B. M. Moudgil, Humana Press, Totowa, NJ, 2010, pp. 25–37, DOI: 10.1007/978-1-60761-609-2_3.
157 Y. Nakamura, A. Mochida, P. L. Choyke and H. Kobayashi, *Bioconjugate Chem.*, 2016, **27**, 2225–2238.
158 Q. Sun, T. Ojha, F. Kiessling, T. Lammers and Y. Shi, *Biomacromolecules*, 2017, **18**, 1449–1459.
159 Y.-R. Zhang, R. Lin, H.-J. Li, W.-l. He, J.-Z. Du and J. Wang, *WIREs Nanomed. Nanobiotechnol.*, 2019, **11**, e1519.
160 Z. Zhang, H. Wang, T. Tan, J. Li, Z. Wang and Y. Li, *Adv. Funct. Mater.*, 2018, **28**, 1801840.
161 V. Mohan, A. Das and I. Sagi, *Semin. Cancer Biol.*, 2020, **62**, 192–200.
162 M. J. Ernsting, M. Murakami, A. Roy and S.-D. Li, *J. Controlled Release*, 2013, **172**, 782–794.
163 X. Cun, J. Chen, M. Li, X. He, X. Tang, R. Guo, M. Deng, M. Li, Z. Zhang and Q. He, *ACS Appl. Mater. Interfaces*, 2019, **11**, 39545–39559.
164 L. Tang, Y. Yin, Z. Zhang, C. Fu, Y. Cao, H. Liu, J. Feng, J. Gao, J. Shang and W. Wang, *Chem. Eng. J.*, 2024, **493**, 152590.

165 Y. Hu, G. Shan, K. A. Rauf, Y. Xiaoye, J. Jianbo, X. Yanwei and G. Zhai, *Expert Opin. Drug Delivery*, 2022, **19**, 221–234.
166 X. Cun, M. Li, S. Wang, Y. Wang, J. Wang, Z. Lu, R. Yang, X. Tang, Z. Zhang and Q. He, *Nanoscale*, 2018, **10**, 9935–9948.
167 X. Shen, D. Pan, Q. Gong, Z. Gu and K. Luo, *Bioact. Mater.*, 2024, **32**, 445–472.
168 Y. Wang, L. Shi, W. Wu, G. Qi, X. Zhu and B. Liu, *Adv. Funct. Mater.*, 2021, **31**, 2010241.
169 P. K. Working, M. S. Newman, S. K. Huang, E. Mayhew, J. Vaage and D. D. Lasic, *J. Liposome Res.*, 1994, **4**, 667–687.
170 Y. Barenholz, *J. Controlled Release*, 2012, **160**, 117–134.
171 J. Voigt, J. Christensen and V. P. Shastri, *Proc. Natl. Acad. Sci. U. S. A.*, 2014, **111**, 2942–2947.
172 P. Zhang, D. Chen, L. Li and K. Sun, *J. Nanobiotechnol.*, 2022, **20**, 31.
173 X. Chen, L. Liu and C. Jiang, *Acta Pharm. Sin. B*, 2016, **6**, 261–267.
174 Y. Liang, J. Wu, Y. Yan, Y. Wang, H. Zhao, X. Wang, S. Chang and S. Li, *Int. J. Mol. Sci.*, 2024, **25**, 9779.
175 F. Veider, E. Sanchez Armengol and A. Bernkop-Schnürch, *Small*, 2024, **20**, 2304713.
176 H.-X. Wang, Z.-Q. Zuo, J.-Z. Du, Y.-C. Wang, R. Sun, Z.-T. Cao, X.-D. Ye, J.-L. Wang, K. W. Leong and J. Wang, *Nano Today*, 2016, **11**, 133–144.
177 D. Y. Kwoh, C. C. Coffin, C. P. Lollo, J. Jovenal, M. G. Banaszczyk, P. Mullen, A. Phillips, A. Amini, J. Fabrycki, R. M. Bartholomew, S. W. Brostoff and D. J. Carlo, *Biochim. Biophys. Acta, Gene Struct. Expression*, 1999, **1444**, 171–190.
178 J. Dai, S. Zou, Y. Pei, D. Cheng, H. Ai and X. Shuai, *Biomaterials*, 2011, **32**, 1694–1705.
179 Z. Zhou, Y. Shen, J. Tang, M. Fan, E. A. Van Kirk, W. J. Murdoch and M. Radosz, *Adv. Funct. Mater.*, 2009, **19**, 3580–3589.
180 R. Kempaiah and Z. Nie, *J. Mater. Chem. B*, 2014, **2**, 2357–2368.
181 M. C. Arno, M. Inam, A. C. Weems, Z. Li, A. L. A. Binch, C. I. Platt, S. M. Richardson, J. A. Hoyland, A. P. Dove and R. K. O'Reilly, *Nat. Commun.*, 2020, **11**, 1420.
182 Q. Lu, H. Yu, T. Zhao, G. Zhu and X. Li, *Nanoscale*, 2023, **15**, 13202–13223.
183 W. Jia, Y. Wang, R. Liu, X. Yu and H. Gao, *Adv. Funct. Mater.*, 2021, **31**, 2009765.
184 R. Agarwal, V. Singh, P. Jurney, L. Shi, S. V. Sreenivasan and K. Roy, *Proc. Natl. Acad. Sci. U. S. A.*, 2013, **110**, 17247–17252.
185 V. P. Chauhan, T. Stylianopoulos, J. D. Martin, Z. Popović, O. Chen, W. S. Kamoun, M. G. Bawendi, D. Fukumura and R. K. Jain, *Nat. Nanotechnol.*, 2012, **7**, 383–388.
186 S.-P. R. Chen, Z. Jia, V. A. Bobrin and M. J. Monteiro, *Biomacromolecules*, 2020, **21**, 133–142.
187 C. Kinnear, T. L. Moore, L. Rodriguez-Lorenzo, B. Rothen-Rutishauser and A. Petri-Fink, *Chem. Rev.*, 2017, **117**, 11476–11521.
188 V. A. Bobrin, S. E. Sharma-Brymer and M. J. Monteiro, *ACS Nano*, 2025, **19**, 3054–3084.
189 V. A. Bobrin, Y. Lin, J. He, Y. Qi, W. Gu and M. J. Monteiro, *Biomacromolecules*, 2020, **21**, 4457–4468.
190 G. J. Doherty and H. T. McMahon, *Annu. Rev. Biochem.*, 2009, **78**, 857–902.
191 R. S. Flannagan, V. Jaumouillé and S. Grinstein, *Annu. Rev. Pathol.: Mech. Dis.*, 2012, **7**, 61–98.
192 M. Kirkham and R. G. Parton, *Biochim. Biophys. Acta, Mol. Cell Res.*, 2005, **1745**, 273–286.
193 D. Zhang, B. Sun, J. Wang, S.-P. R. Chen, V. A. Bobrin, Y. Gu, C. K. Ng, W. Gu and M. J. Monteiro, *Biomacromolecules*, 2024, **25**, 5260–5272.
194 W. Jia, R. Liu, Y. Wang, C. Hu, W. Yu, Y. Zhou, L. Wang, M. Zhang, H. Gao and X. Gao, *Acta Pharm. Sin. B*, 2022, **12**, 3354–3366.
195 F. Tong, Y. Wang, Y. Xu, Y. Zhou, S. He, Y. Du, W. Yang, T. Lei, Y. Song, T. Gong and H. Gao, *Nat. Commun.*, 2024, **15**, 10382.
196 R. Lin, J. Yan, B. Gong, F. Tong, Y. Song, X. Xia, H. Hu, Y. Wang, Y. Zhou, T. Gong, M. Shevtsov and H. Gao, *Adv. Funct. Mater.*, 2024, **34**, 2405051.
197 Z. Cao, J. Liu and X. Yang, *Exploration*, 2024, **4**, 20230037.
198 Y. Wang, M. Qiu, M. Won, E. Jung, T. Fan, N. Xie, S.-G. Chi, H. Zhang and J. S. Kim, *Coord. Chem. Rev.*, 2019, **400**, 213041.
199 Z. Li, X. Shan, Z. Chen, N. Gao, W. Zeng, X. Zeng and L. Mei, *Adv. Sci.*, 2021, **8**, 2002589.
200 S. W. Choi, K. Woo-Sik and J. H. Kim, *J. Dispersion Sci. Technol.*, 2003, **24**, 475–487.
201 Q. Dai, Y. Yan, C.-S. Ang, K. Kempe, M. M. J. Kamphuis, S. J. Dodds and F. Caruso, *ACS Nano*, 2015, **9**, 2876–2885.
202 P. Patel, A. Hanini, A. Shah, D. Patel, S. Patel, P. Bhatt and Y. V. Pathak, in *Surface Modification of Nanoparticles for Targeted Drug Delivery*, ed. Y. V. Pathak, Springer International Publishing, Cham, 2019, pp. 19–31, DOI: 10.1007/978-3-030-06115-9_2.
203 K. T. K. Reddy and A. S. Reddy, *Cell., Mol. Biomed. Rep.*, 2025, **5**, 13–27.
204 V. S. Verma, A. Pandey, A. K. Jha, H. K. R. Badwaik, A. Alexander and Ajazuddin, *Appl. Biochem. Biotechnol.*, 2024, **196**, 7325–7361.
205 Z. Zhen, W. Tang, H. Chen, X. Lin, T. Todd, G. Wang, T. Cowger, X. Chen and J. Xie, *ACS Nano*, 2013, **7**, 4830–4837.
206 D. Nikitovic, E. Kukovyakina, A. Berdiaki, A. Tzanakakis, A. Luss, E. Vlaskina, A. Yagolovich, A. Tsatsakis and A. Kuskov, *Cancer*, 2024, **16**, 3768.
207 M. Sanati, A. R. Afshari, S. Aminyavari, P. Kesharwani, T. Jamialahmadi and A. Sahebkar, *J. Drug Delivery Sci. Technol.*, 2023, **84**, 104562.
208 F. Danhier, B. Vroman, N. Lecouturier, N. Crokart, V. Pourcelle, H. Freichels, C. Jérôme, J. Marchand-Brynaert, O. Feron and V. Préat, *J. Controlled Release*, 2009, **140**, 166–173.

209 E. Ruoslahti and M. D. Pierschbacher, *Science*, 1987, **238**, 4826.
210 F. Wang, Y. Li, Y. Shen, A. Wang, S. Wang and T. Xie, *Int. J. Mol. Sci.*, 2013, **14**, 13447–13462.
211 F. Danhier, A. Le Breton and V. Préat, *Mol. Pharm.*, 2012, **9**, 2961–2973.
212 Y. Gu, V. Bobrin, D. Zhang, B. Sun, C. K. Ng, S.-P. R. Chen, W. Gu and M. J. Monteiro, *Cancers*, 2023, **15**, 234.
213 X. Li, J. Guo, J. Asong, M. A. Wolfert and G.-J. Boons, *J. Am. Chem. Soc.*, 2011, **133**, 11147–11153.
214 T. Jiang, Y. Zhan, J. Ding, Z. Song, Y. Zhang, J. Li and T. Su, *ChemMedChem*, 2024, **19**, e202400410.
215 Y. Qu, B. Chu, X. Wei, Y. Chen, Y. Yang, D. Hu, J. Huang, F. Wang, M. Chen, Y. Zheng and Z. Qian, *Adv. Mater.*, 2022, **34**, 2107883.
216 Y. Liu, J. Luo, X. Chen, W. Liu and T. Chen, *Nano-Micro Lett.*, 2019, **11**, 100.
217 R. H. Fang, C.-M. J. Hu, B. T. Luk, W. Gao, J. A. Copp, Y. Tai, D. E. O'Connor and L. Zhang, *Nano Lett.*, 2014, **14**, 2181–2188.
218 A. Gupta, S. Soni, N. Chauhan, M. Khanuja and U. Jain, *J. Controlled Release*, 2022, **349**, 97–108.
219 S. Zhang, C. Zhu, W. Huang, H. Liu, M. Yang, X. Zeng, Z. Zhang, J. Liu, J. Shi, Y. Hu, X. Shi and Z.-H. Wang, *J. Controlled Release*, 2023, **360**, 514–527.
220 X. Zhou, X. Huang, B. Wang, L. Tan, Y. Zhang and Y. Jiao, *Chem. Eng. J.*, 2021, **408**, 127897.
221 Y. Opoku-Damoah, R. Zhang, H. T. Ta and Z. P. Xu, *Exploration*, 2022, **2**, 20210181.
222 L. Yu, P. Hu and Y. Chen, *Adv. Mater.*, 2018, **30**, 1801964.
223 M. M. Wan, H. Chen, Z. Da Wang, Z. Y. Liu, Y. Q. Yu, L. Li, Z. Y. Miao, X. W. Wang, Q. Wang, C. Mao, J. Shen and J. Wei, *Adv. Sci.*, 2021, **8**, 2002525.
224 R. Grifantini, M. Taranta, L. Gherardini, I. Naldi, M. Parri, A. Grandi, A. Giannetti, S. Tombelli, G. Lucarini, L. Ricotti, S. Campagnoli, E. De Camilli, G. Pelosi, F. Baldini, A. Menciassi, G. Viale, P. Pileri and C. Cinti, *J. Controlled Release*, 2018, **280**, 76–86.
225 R. Tietze, J. Zaloga, H. Unterweger, S. Lyer, R. P. Friedrich, C. Janko, M. Pöttler, S. Dürr and C. Alexiou, *Biochem. Biophys. Res. Commun.*, 2015, **468**, 463–470.
226 J. Huang, Y. Li, A. Orza, Q. Lu, P. Guo, L. Wang, L. Yang and H. Mao, *Adv. Funct. Mater.*, 2016, **26**, 3818–3836.
227 V. V. Mody, A. Cox, S. Shah, A. Singh, W. Bevins and H. Parihar, *Appl. Nanosci.*, 2014, **4**, 385–392.
228 A. J. Willis, S. P. Pernal, Z. A. Gaertner, S. S. Lakka, M. E. Sabo, F. M. Creighton and H. H. Engelhard, *Int. J. Nanomed.*, 2020, **15**, 4105–4123.
229 M. Medina-Sánchez, X. Haifeng and O. G. Schmidt, *Ther. Delivery*, 2018, **9**, 303–316.
230 D. Shao, J. Li, X. Zheng, Y. Pan, Z. Wang, M. Zhang, Q.-X. Chen, W.-F. Dong and L. Chen, *Biomaterials*, 2016, **100**, 118–133.
231 Y. Zhu, Y. Song, Z. Cao, L. Dong, Y. Lu, X. Yang and J. Wang, *Adv. Funct. Mater.*, 2021, **31**, 2103655.
232 M. Liu, X. Hou and D. Wang, *Sci. China Mater.*, 2024, **67**, 2373–2375.
233 J. Annamalai, S. B. Ummalyma, A. Pandey and T. Bhaskar, *Environ. Sci. Pollut. Res.*, 2021, **28**, 49362–49382.
234 L. Zhang, J. J. Abbott, L. Dong, B. E. Kratochvil, D. Bell and B. J. Nelson, *Appl. Phys. Lett.*, 2009, **94**, 064107.
235 C. Mukai, M. Bergkvist, J. L. Nelson and A. J. Travis, *Chem. Biol.*, 2009, **16**, 1013–1020.
236 V. Magdanz and O. G. Schmidt, *Expert Opin. Drug Delivery*, 2014, **11**, 1125–1129.
237 V. M. Moreno, E. Álvarez, I. Izquierdo-Barba, A. Baeza, J. Serrano-López and M. Vallet-Regí, *Adv. Mater. Interfaces*, 2020, **7**, 1901942.
238 S. Wang, Y. Jiang, Z. Qian, L. Ren, J. Wang, Y. Liu, Y. Li, J. Li, K. Qu, F. Wang, H. Wu, F. Yang, Y. Zhang, Y. Gao and L. Wang, *Chem. Eng. J.*, 2024, **488**, 151072.
239 M. Ijaz, I. Hasan, T. H. Chaudhry, R. Huang, L. Zhang, Z. Hu, Q. Tan and B. Guo, *J. Nanobiotechnol.*, 2024, **22**, 510.
240 S. Zheng, X. Li and S. Guo, *BMEMat*, 2024, **2**, e12110.
241 Q. Jiang, J. He, H. Zhang, H. Chi, Y. Shi and X. Xu, *Mater. Today Bio*, 2024, **27**, 101119.
242 Y. Zhang, S.-H. Ho, B. Li, G. Nie and S. Li, *Med. Res. Rev.*, 2020, **40**, 1084–1102.
243 S. Sakai, C. Iwata, H. Y. Tanaka, H. Cabral, Y. Morishita, K. Miyazono and M. R. Kano, *J. Controlled Release*, 2016, **230**, 109–115.
244 F. Klemm and J. A. Joyce, *Trends Cell Biol.*, 2015, **25**, 198–213.
245 B. Diop-Frimpong, V. P. Chauhan, S. Krane, Y. Boucher and R. K. Jain, *Proc. Natl. Acad. Sci. U. S. A.*, 2011, **108**, 2909–2914.
246 K. L. Schaefer, J. A. Porter, B. R. Morand and M. Rudis, *Ann. Pharmacother.*, 1996, **30**, 625–636.
247 H. Takagi, K. Kaji, N. Nishimura, K. Ishida, H. Ogawa, H. Takaya, H. Kawaratani, K. Moriya, T. Namisaki, T. Akahane, A. Mitoro and H. Yoshiji, *Cells*, 2021, **10**, 575.
248 F. Xu, X. Huang, Y. Wang and S. Zhou, *Adv. Mater.*, 2020, **32**, 1906745.
249 R. Pavan, S. Jain, Shraddha and A. Kumar, *Biotechnol. Res. Int.*, 2012, **2012**, 976203.
250 A. Parodi, S. G. Haddix, N. Taghipour, S. Scaria, F. Taraballi, A. Cevenini, I. K. Yazdi, C. Corbo, R. Palomba, S. Z. Khaled, J. O. Martinez, B. S. Brown, L. Isenhart and E. Tasciotti, *ACS Nano*, 2014, **8**, 9874–9883.
251 M. Zhang, Y. Chen, Y. Li, Y. Zhao, B. Lv, J. Cao, B. Yu and H. Cong, *Chin. Chem. Lett.*, 2025, 111588, DOI: 10.1016/j.cclet.2025.111588.
252 H. Shen, J. You, G. Zhang, A. Ziemys, Q. Li, L. Bai, X. Deng, D. R. Erm, X. Liu, C. Li and M. Ferrari, *Adv. Healthcare Mater.*, 2012, **1**, 84–89.
253 Y. Tian, T. Cheng, F. Sun, Y. Zhou, C. Yuan, Z. Guo and Z. Wang, *Adv. Colloid Interface Sci.*, 2024, **326**, 103124.
254 L. Li, T. L. M. ten Hagen, M. Hossann, R. Süss, G. C. van Rhoon, A. M. M. Eggermont, D. Haemmerich and G. A. Koning, *J. Controlled Release*, 2013, **168**, 142–150.

255 Z. Deng, Y. Xiao, M. Pan, F. Li, W. Duan, L. Meng, X. Liu, F. Yan and H. Zheng, *J. Controlled Release*, 2016, **243**, 333–341.
256 R. van der Meel, E. Sulheim, Y. Shi, F. Kiessling, W. J. M. Mulder and T. Lammers, *Nat. Nanotechnol.*, 2019, **14**, 1007–1017.
257 R. K. Jain and T. Stylianopoulos, *Nat. Rev. Clin. Oncol.*, 2010, **7**, 653–664.
258 E. Frohlich, *Int. J. Nanomed.*, 2012, **7**, 5577–5591.
259 O. Lieleg, R. M. Baumgärtel and A. R. Bausch, *Biophys. J.*, 2009, **97**, 1569–1577.
260 L. E. Roode, H. Brighton, T. Bo, J. L. Perry, M. C. Parrott, F. Kersey, J. C. Luft, J. E. Bear, J. M. DeSimone and I. J. Davis, *Nanomedicine*, 2016, **12**, 1053–1062.
261 Y. Lee, T. Ishii, H. Cabral, H. J. Kim, J.-H. Seo, N. Nishiyama, H. Oshima, K. Osada and K. Kataoka, *Angew. Chem., Int. Ed.*, 2009, **48**, 5309–5312.
262 J. Zhang, Y. Li, L. Wang, C. Zhang and H. He, *Catal. Sci. Technol.*, 2015, **5**, 2305–2313.
263 J. Cui, Y. Yan, Y. Wang and F. Caruso, *Adv. Funct. Mater.*, 2012, **22**, 4718–4723.
264 Z. Guo, J. Sui, M. Ma, J. Hu, Y. Sun, L. Yang, Y. Fan and X. Zhang, *J. Controlled Release*, 2020, **326**, 350–364.
265 Y. Gu, Y. Zhong, F. Meng, R. Cheng, C. Deng and Z. Zhong, *Biomacromolecules*, 2013, **14**, 2772–2780.
266 J. Liu, Y. Huang, A. Kumar, A. Tan, S. Jin, A. Mozhi and X.-J. Liang, *Biotechnol. Adv.*, 2014, **32**, 693–710.
267 G. He, S. Chen, Y. Xu, Z. Miao, Y. Ma, H. Qian, Y. Lu and Z. Zha, *Mater. Horiz.*, 2019, **6**, 711–716.
268 H. Deng, X. Zhao, J. Liu, L. Deng, J. Zhang, J. Liu and A. Dong, *J. Mater. Chem. B*, 2015, **3**, 9397–9408.
269 K. Luo, Y. Lian, M. Zhang, H. Yu, G. Wang and J. Li, *Chem. Eng. J.*, 2021, **412**, 128659.
270 Y. Huang, Z. Tang, X. Zhang, H. Yu, H. Sun, X. Pang and X. Chen, *Biomacromolecules*, 2013, **14**, 2023–2032.
271 Z.-Y. Li, Y. Liu, J.-J. Hu, Q. Xu, L.-H. Liu, H.-Z. Jia, W.-H. Chen, Q. Lei, L. Rong and X.-Z. Zhang, *ACS Appl. Mater. Interfaces*, 2014, **6**, 14568–14575.
272 L. Zhu, P. Kate and V. P. Torchilin, *ACS Nano*, 2012, **6**, 3491–3498.
273 H.-X. Wang, X.-Z. Yang, C.-Y. Sun, C.-Q. Mao, Y.-H. Zhu and J. Wang, *Biomaterials*, 2014, **35**, 7622–7634.
274 L. Zhu, F. Perche, T. Wang and V. P. Torchilin, *Biomaterials*, 2014, **35**, 4213–4222.
275 T. L. Andresen, J. Davidsen, M. Begtrup, O. G. Mouritsen and K. Jørgensen, *J. Med. Chem.*, 2004, **47**, 1694–1703.
276 Q. Zhou, S. Shao, J. Wang, C. Xu, J. Xiang, Y. Piao, Z. Zhou, Q. Yu, J. Tang, X. Liu, Z. Gan, R. Mo, Z. Gu and Y. Shen, *Nat. Nanotechnol.*, 2019, **14**, 799–809.
277 H. Chen, Q. Guo, Y. Chu, C. Li, Y. Zhang, P. Liu, Z. Zhao, Y. Wang, Y. Luo, Z. Zhou, T. Zhang, H. Song, X. Li, C. Li, B. Su, H. You, T. Sun and C. Jiang, *Biomaterials*, 2022, **287**, 121599.
278 F. Perche, S. Biswas, T. Wang, L. Zhu and V. P. Torchilin, *Angew. Chem., Int. Ed.*, 2014, **53**, 3362–3366.
279 M. Shen, Y. Wang, T. Bing, Y. Tang, X. Liu and Y. Yu, *Adv. Funct. Mater.*, 2023, **33**, 2307013.
280 J.-Y. Gong, Y. Li, P. Wang, X. Peng, R. Xie, W. Wang, Z. Liu, D.-W. Pan, X.-J. Ju and L.-Y. Chu, *ACS Nano*, 2025, **19**, 2345–2361.
281 L. Fang, Z. Zhao, J. Wang, P. Xiao, X. Sun, Y. Ding, P. Zhang, D. Wang and Y. Li, *Acta Pharm. Sin. B*, 2022, **12**, 353–363.
282 A. Yavlovich, S. Brandon, G. Kshitij, B. Robert and A. Puri, *Mol. Membr. Biol.*, 2010, **27**, 364–381.
283 J. L. Vivero-Escoto, I. I. Slowing, C.-W. Wu and V. S. Y. Lin, *J. Am. Chem. Soc.*, 2009, **131**, 3462–3463.
284 L.-C. Hu, Y. Yonamine, S.-H. Lee, W. E. van der Veer and K. J. Shea, *J. Am. Chem. Soc.*, 2012, **134**, 11072–11075.
285 L. Liu and P. Liu, *Front. Mater. Sci.*, 2015, **9**, 211–226.
286 F. Badparvar, A. P. Marjani, R. Salehi and F. Ramezani, *Sci. Rep.*, 2024, **14**, 8567.
287 X. Xu, P. E. Saw, W. Tao, Y. Li, X. Ji, S. Bhasin, Y. Liu, D. Ayyash, J. Rasmussen, M. Huo, J. Shi and O. C. Farokhzad, *Adv. Mater.*, 2017, **29**, 1700141.
288 X. Liu, J. Xiang, D. Zhu, L. Jiang, Z. Zhou, J. Tang, X. Liu, Y. Huang and Y. Shen, *Adv. Mater.*, 2016, **28**, 1743–1752.
289 T. Chi, T. Sang, Y. Wang and Z. Ye, *Bioconjugate Chem.*, 2024, **35**, 1–21.
290 J. Chen, J. Ding, Y. Wang, J. Cheng, S. Ji, X. Zhuang and X. Chen, *Adv. Mater.*, 2017, **29**, 1701170.
291 Z. B. Akkuş-Dağdeviren, A. Fürst, J. David Friedl, M. Tribus and A. Bernkop-Schnürch, *J. Colloid Interface Sci.*, 2023, **629**, 541–553.
292 J. Mu, J. Lin, P. Huang and X. Chen, *Chem. Soc. Rev.*, 2018, **47**, 5554–5573.
293 X. Kang, F. Bu, W. Feng, F. Liu, X. Yang, H. Li, Y. Yu, G. Li, H. Xiao and X. Wang, *Adv. Mater.*, 2022, **34**, 2206765.
294 Y. Zeng, M. Jingwen, Z. Yonghua, X. Xinyi, Z. Qi, L. Jimin and X. Chen, *Int. J. Nanomed.*, 2018, **13**, 6551–6574.
295 Y. Li, L. Zhao and X.-F. Li, *Technol Cancer Res. Treat.*, 2021, **20**, DOI: 10.1177/15330338211036304.
296 M.-Z. Zou, W.-L. Liu, H.-S. Chen, X.-F. Bai, F. Gao, J.-J. Ye, H. Cheng and X.-Z. Zhang, *Natl. Sci. Rev.*, 2021, **8**, nwaa160.
297 Z. Fang, S. Pan, P. Gao, H. Sheng, L. Li, L. Shi, Y. Zhang and X. Cai, *Int. J. Pharm.*, 2020, **575**, 118841.
298 J. Liao, H. Peng, C. Liu, D. Li, Y. Yin, B. Lu, H. Zheng and Q. Wang, *Mater. Sci. Eng., C*, 2021, **118**, 111527.
299 X. Zhang, C. Zhang, M. Cheng, Y. Zhang, W. Wang and Z. Yuan, *Nano Res.*, 2019, **12**, 2815–2826.
300 C. Zhang, J. Chen, Y. Song, J. Luo, P. Jin, X. Wang, L. Xin, F. Qiu, J. Yao, G. Wang and P. Huang, *ACS Appl. Mater. Interfaces*, 2022, **14**, 2587–2596.
301 N. Qiu, J. Gao, Q. Liu, J. Wang and Y. Shen, *Biomacromolecules*, 2018, **19**, 2308–2319.
302 R. Sun, Y. Zhang, X. Lin, Y. Piao, T. Xie, Y. He, J. Xiang, S. Shao, Q. Zhou, Z. Zhou, J. Tang and Y. Shen, *Angew. Chem., Int. Ed.*, 2023, **62**, e202217408.
303 Y. Wu, J. Zheng, Q. Zeng, T. Zhang and D. Xing, *Nano Res.*, 2020, **13**, 2399–2406.

304 M. Zhou, H. Huang, D. Wang, H. Lu, J. Chen, Z. Chai, S. Q. Yao and Y. Hu, *Nano Lett.*, 2019, **19**, 3671–3675.
305 H. Yang, Y. Li, T. Li, M. Xu, Y. Chen, C. Wu, X. Dang and Y. Liu, *Sci. Rep.*, 2014, **4**, 7072.
306 O. Boussif, F. Lezoualc'h, M. A. Zanta, M. D. Mergny, D. Scherman, B. Demeneix and J. P. Behr, *Proc. Natl. Acad. Sci. U. S. A.*, 1995, **92**, 7297–7301.
307 A. Akinc, M. Thomas, A. M. Klibanov and R. Langer, *J. Gene Med.*, 2005, **7**, 657–663.
308 W. Yang, K. Yan, Y. Feng and X. Zhao, *Eur. J. Pharm. Biopharm.*, 2024, **205**, 114560.
309 J. Li, X. Yu, Y. Wang, Y. Yuan, H. Xiao, D. Cheng and X. Shuai, *Adv. Mater.*, 2014, **26**, 8217–8224.
310 H.-J. Li, J.-Z. Du, J. Liu, X.-J. Du, S. Shen, Y.-H. Zhu, X. Wang, X. Ye, S. Nie and J. Wang, *ACS Nano*, 2016, **10**, 6753–6761.
311 Y. Yu, X. Zhang and L. Qiu, *Biomaterials*, 2014, **35**, 3467–3479.
312 J. J. Rennick, A. P. R. Johnston and R. G. Parton, *Nat. Nanotechnol.*, 2021, **16**, 266–276.
313 R. Rampado, S. Crotti, P. Caliceti, S. Pucciarelli and M. Agostini, *Front. Bioeng. Biotechnol.*, 2020, **8**, 166.